



Apelin protects against abdominal aortic aneurysm and the therapeutic role of neutral endopeptidase resistant apelin analogs

Wang Wang^{a,b,c}, Mengcheng Shen^{b,c}, Conrad Fischer^d, Ratnadeep Basu^{a,b}, Saugata Hazra^{e,f}, Pierre Couvineau^g, Manish Paul^h, Faqi Wang^{a,b}, Sandra Tothⁱ, Doran S. Mixⁱ, Marko Poglitsch^j, Norma P. Gerard^k, Michel Bouvier^g, John C. Vederas^d, Josef M. Penninger^l, Zamaneh Kassiri^{b,c}, and Gavin Y. Oudit^{a,b,c,1}

^aDivision of Cardiology, Department of Medicine, University of Alberta, Edmonton, AB T6G 2G3, Canada; ^bMazankowski Alberta Heart Institute, University of Alberta, Edmonton, AB T6G 2J2, Canada; ^cDepartment of Physiology, University of Alberta, Edmonton, AB T6G 2R7, Canada; ^dDepartment of Chemistry, University of Alberta, Edmonton, AB T6G 2N4, Canada; ^eDepartment of Biotechnology, Indian Institute of Technology, 247667 Roorkee, Uttarakhand, India; ^fCentre for Nanotechnology, Indian Institute of Technology, 247667 Roorkee, Uttarakhand, India; ^gDepartment of Biochemistry and Molecular Medicine, Faculty of Medicine, University of Montreal, Montreal, QC H3C 3J7, Canada; ^hDepartment of Biotechnology, North Orissa University, 757003 Baripada, Odisha, India; ⁱDivision of Vascular Surgery, University of Rochester, Rochester, NY 14642; ^jAttoquant Diagnostics, 1030 Vienna, Austria; ^kBoston Children's Hospital, Beth Israel Deaconess Medical Center, Harvard Medical School, Boston, MA 02115; and ^lDepartment of Medical Genetics, Life Sciences Institute, University of British Columbia, Vancouver, BC V6H 3N1, Canada

Edited by Christine E. Seidman, Howard Hughes Medical Institute, Brigham and Women's Hospital, Harvard Medical School, Boston, MA, and approved May 21, 2019 (received for review January 7, 2019)

Abdominal aortic aneurysm (AAA) remains the second most frequent vascular disease with high mortality but has no approved medical therapy. We investigated the direct role of apelin (APLN) in AAA and identified a unique approach to enhance APLN action as a therapeutic intervention for this disease. Loss of APLN potentiated angiotensin II (Ang II)-induced AAA formation, aortic rupture, and reduced survival. Formation of AAA was driven by increased smooth muscle cell (SMC) apoptosis and oxidative stress in *Apln*^{-/-} aorta and in APLN-deficient cultured murine and human aortic SMCs. Ang II-induced myogenic response and hypertension were greater in *Apln*^{-/-} mice, however, an equivalent hypertension induced by phenylephrine, an α -adrenergic agonist, did not cause AAA or rupture in *Apln*^{-/-} mice. We further identified Ang converting enzyme 2 (ACE2), the major negative regulator of the renin-Ang system (RAS), as an important target of APLN action in the vasculature. Using a combination of genetic, pharmacological, and modeling approaches, we identified neutral endopeptidase (NEP) that is up-regulated in human AAA tissue as a major enzyme that metabolizes and inactivates APLN-17 peptide. We designed and synthesized a potent APLN-17 analog, APLN-NMeLeu9-A2, that is resistant to NEP cleavage. This stable APLN analog ameliorated Ang II-mediated adverse aortic remodeling and AAA formation in an established model of AAA, high-fat diet (HFD) in *Ldlr*^{-/-} mice. Our findings define a critical role of APLN in AAA formation through induction of ACE2 and protection of vascular SMCs, whereas stable APLN analogs provide an effective therapy for vascular diseases.

as well as many other cardiovascular pathologies (5). Meanwhile, the APLN pathway has emerged as a major peptide hormone pathway capable of exerting beneficial metabolic and cardiovascular effects (6–10). APLN is widely expressed in mammals including in endothelial cells and VSMCs (11, 12). The APLN precursor peptide is processed into several peptides including APLN-17 (13, 14), the most potent APLN peptide in the cardiovascular system. ACE2 is the major negative regulator of the RAS and converts Ang II into the vasculoprotective peptide, Ang 1–7 (5, 15–17).

In this study, we defined a marked susceptibility of the abdominal aorta lacking APLN to the development of AAA in response to Ang II. This was driven by reduced ACE2 levels, deficiency, oxidative stress, and apoptotic cell death of VSMCs. We identified NEP as a key enzyme that degrades and inactivates the active APLN-17 peptide, developed a stable APLN-17 analog resistant to NEP degradation, and established the

Significance

Vascular diseases remain a major health burden, and AAAs lack effective medical therapy. We demonstrate a seminal role for APLN in AAA pathogenesis based on loss-of-function and gain-of-function approaches and included human vascular SMCs and AA tissue obtained from patients. We identified NEP as a dominant inactivating enzyme for native APLN-17. This allowed us to design and synthesize a stable and bioactive APLN analog resistant to NEP degradation that showed profound therapeutic effects against AAA. Our study clearly defines the APLN pathway as a central node in the pathogenesis of AAA and elucidate a therapeutic strategy of enhancing the APLN pathway by using a stable APLN analog to treat AAA.

apelin | ACE2 | neutral endopeptidase | aneurysm | angiotensin II

AAA is defined as an enlargement of the AA to >1.5-fold of its normal size, and the overall AAA prevalence is estimated to be 6% in men and 1.6% in women (1–3). The asymptomatic nature of AAA makes the diagnosis extremely challenging, whereas ruptured AAA accounts for ~15,000 deaths in the United States annually (4). Open surgical repair or endovascular repair are the only treatment options for patients with advanced AAA. Importantly, several modes of medical therapy have failed to provide benefits in patients with AAAs (1–3). Therefore, a better understanding of the cellular dysregulation and signaling networks responsible for the formation and progression of AAA is necessary for the discovery of novel and effective therapies.

Homeostasis of endothelial cells and vascular SMCs (VSMCs), the major cell populations of the vascular wall, play a crucial role in AAA development and disease progression. Activation of the RAS and production of Ang II lead to adverse vascular remodeling

Author contributions: W.W., J.C.V., Z.K., and G.Y.O. designed research; W.W., M.S., C.F., S.H., P.C., M. Paul, F.W., M. Poglitsch, M.B., and G.Y.O. performed research; W.W., C.F., S.T., D.S.M., N.P.G., J.C.V., and J.M.P. contributed new reagents/analytic tools; W.W., M.S., C.F., R.B., S.H., P.C., M. Paul, F.W., S.T., D.S.M., M. Poglitsch, M.B., Z.K., and G.Y.O. analyzed data; and W.W. and G.Y.O. wrote the paper.

Conflict of interest statement: Our apelin analogs have been submitted for patenting.

This article is a PNAS Direct Submission.

This open access article is distributed under [Creative Commons Attribution-NonCommercial-NoDerivatives License 4.0 \(CC BY-NC-ND\)](https://creativecommons.org/licenses/by-nc-nd/4.0/).

¹To whom correspondence may be addressed. Email: gavin.oudit@ualberta.ca.

This article contains supporting information online at www.pnas.org/lookup/suppl/doi:10.1073/pnas.1900152116/-DCSupplemental.

Published online June 12, 2019.

therapeutic effects of this developed stable APLN analog in preventing vascular disease and formation of AAA.

Results

Loss of APLN Enhances Susceptibility to AAA. Histological analyses of human AAA revealed severely disrupted medial structure characterized by fragmented elastin fibers associated with the loss of SMCs and increased cell death in AAA specimens compared with the nondiseased aorta (NDA) (Fig. 1 *A* and *B* and *SI Appendix*, Fig. S1*A* and Table S1). These structural changes in the aneurysmal aorta were associated with increased APLN levels compared with nonaneurysmal aorta (Fig. 1 *C* and *D* and *SI Appendix*, Fig. S1*B*) and APLN was increased in Ang II-infused wild-type (WT) (*Apln*^{+/-}) mice aorta (Fig. 1 *E* and *F*). A similar pattern was also seen in the thoracic aorta from patients with bicuspid aortic valve and aortopathy (*SI Appendix*, Fig. S2*A*).

Ang II is a well-known mediator of adverse vascular remodeling and is widely used in AAA models (18–21). The up-regulation of APLN levels in the diseased aorta suggest that the APLN pathway is responsive to disease. To determine the role of APLN in AAA, we tested the effects of Ang II in WT (*Apln*^{+/-}) and APLN knockout (*Apln*^{-/-}) mice. Four weeks of Ang II infusion resulted

in high incidence of severe AAA in the *Apln*^{-/-} but not in parallel WT mice (Fig. 2*A*). The AAA in *Apln*^{-/-} mice was associated with aortic dissection, intramural hematoma, and increased mortality due to aortic rupture (Fig. 2*B* and *C*). Among the 23 *Apln*^{-/-} mice that received Ang II, 5 died from AAA rupture, 18 survived, and 12 of the survivors developed AAA (Fig. 2*A–C*). Vascular ultrasound imaging showed progressive greater dilation, localized aneurysm formation, and decreased compliance (aortic expansion index) in the abdominal aorta of Ang II-infused *Apln*^{-/-} compared with *Apln*^{+/-} mice, whereas no difference was observed between the genotypes at baseline (Fig. 2*D*). Consistent with the phenotypic changes in the abdominal aorta, thoracic aorta also displayed adverse remodeling in *Apln*^{-/-} compared with *Apln*^{+/-} mice (*SI Appendix*, Fig. S2*B*). Histological analyses confirmed disruption of the elastin lamellae in the aortic media and excess fibrotic deposition in the adventitia in *Apln*^{-/-} mice compared with the uniform thickening of the aortic wall in *Apln*^{+/-} mice in response to Ang II (Fig. 2*E*). Overall, our findings demonstrate that APLN is a major determinant in the pathogenesis of AAA.

APLN Deficiency Promotes Ang II-Induced Hypertension and VSMC Stress. We next explored the mechanism for the enhanced susceptibility of APLN-deficient mice to Ang II-induced AAA. We

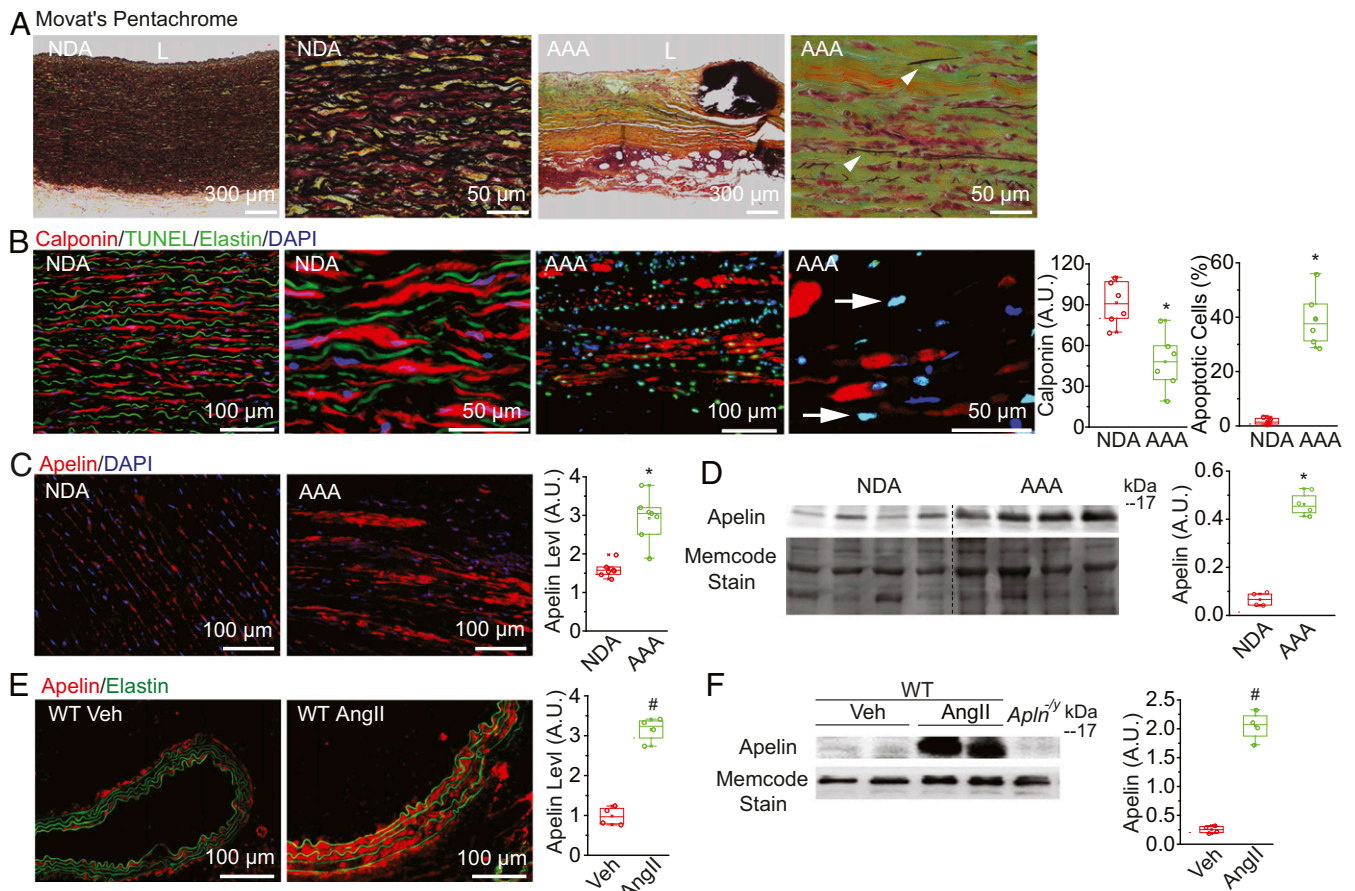


Fig. 1. Up-regulation of APLN levels in vascular disease. (*A* and *B*) Adverse structural remodeling in surgical resected AAA specimens from patients as revealed by Movat's pentachrome (*A*) and anti-calponin staining to visualize SMCs (red, *B*) of NDA and AAA. The arrow heads in AAA images point to elastin fiber fragments. L = aortic lumen. (*B*) Elastin fiber autofluorescence appears green. DAPI staining (blue) was used to visualize the nuclei. Averaged SMC content (calponin-positive staining), and apoptotic SMCs (positive for TUNEL in green and DAPI staining) in the NDA and AAA are shown as boxes with scatter plots on the right. *n* = 6/group. The arrows in AAA images point to apoptotic cells. (*C*) Immunostaining for APLN (red) with DAPI nuclear staining (blue), and Western blots for APLN (*D*) in NDA and AAA specimens with averaged quantification of APLN levels shown in boxes with scatter plots; *n* = 7/group in *C*, *n* = 4/group in *D*. (*E*) Immunostaining for APLN (red) with DAPI nuclear staining (blue), and Western blots (*F*) in abdominal aorta from WT mice receiving saline as vehicle (Veh) or Ang II for 4 wk (1.5 mg/kg/d) with averaged quantification of APLN levels shown in boxes and scatter plots; *n* = 4/group. **P* < 0.05 compared with the NDA group; #*P* < 0.05 compared with the Veh group; A.U., arbitrary units.

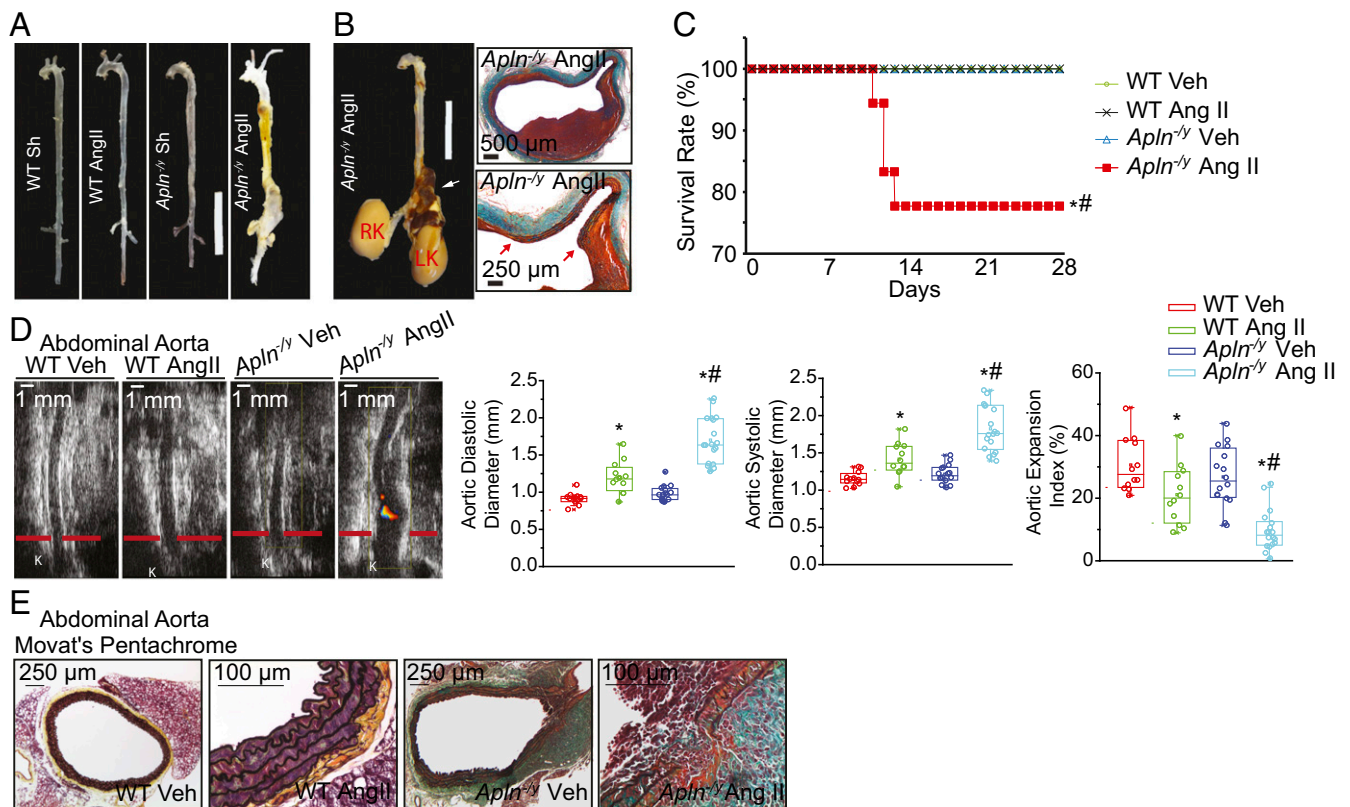


Fig. 2. APLN deficiency increases susceptibility to AAA and vascular SMC death. (A and B) Representative pictures of the whole aorta from all groups showing the presence of aneurysms (A), aortic dissection, and rupture (B) leading to hemorrhage in the peritoneal cavity in the *Apln*^{-/-}-Ang II group. The white arrow points to a hemorrhage. RK = right kidney, LK = left kidney, and the red arrows point to ruptured ends of elastin lamellae. (C) Kaplan Meir survival curve showing mortality due to aortic rupture assessed by logarithm-rank testing. *n* = 12–18/group. (D) Ultrasonographic B-mode images of the AA in Ang II-infused WT and *Apln*^{-/-} mice. “K” indicates the top of the left kidney as a reference, and the red lines show where measurements of aortic diameter were obtained (suprarenal). Averaged aortic systolic and diastolic diameters and aortic systolic expansion index of AA in vehicle- or Ang II-infused groups are shown. *n* = 12–18/group. (E) Histological analysis (Movat’s pentachrome staining) showing disruption of the elastin lamellae in the medial aortic wall with fibrotic deposition in *Apln*^{-/-} mice compared with the uniform thickening of the aortic wall in WT mice exposed to Ang II. **P* < 0.05 compared with the Veh group; #*P* < 0.05 compared with the WT-Ang II group.

determined the impact of *Apln* deficiency on vascular function and showed stronger Ang II-induced vasoconstriction in *Apln*^{-/-} mesenteric resistance arteries compared with *Apln*^{+/-} arteries associated with marked suppression of basal phospho-eNOS (Ser1177) levels (Fig. 3A and *SI Appendix*, Fig. S3A and B). In vivo telemetric blood pressure measurement demonstrated that, although baseline blood pressure was equivalent in both genotypes, Ang II resulted in a greater increase in mean arterial blood pressure (MABP) during the day and night in *Apln*^{-/-} compared with parallel *Apln*^{+/-} mice (Fig. 3B). In contrast to Ang II effects, the intrinsic myogenic response and maximal vasoconstriction in response to high extracellular potassium was equivalent in both genotypes (*SI Appendix*, Fig. S3C–E). To test whether the Ang II-induced higher blood pressure in *Apln*^{-/-} mice accounted for AAA formation, we used another hypertensive agent, phenylephrine (PE), to induce the same degree of hypertension. Interestingly, no AAA was observed in either *Apln*^{-/-} mice or their parallel control *Apln*^{+/-} mice after 4 wk of PE infusion (*SI Appendix*, Fig. S4). These results demonstrate that the APLN-deficient vasculature is intrinsically susceptible to the adverse effects of Ang II-induced vascular remodeling.

We investigated the cellular basis for the enhanced susceptibility to AAA formation in *Apln*^{-/-} mice and found reduced VSMC density, increased apoptotic cell death, and cleaved caspase 3 levels following 2 wk (*SI Appendix*, Fig. S5A) and 4 wk of Ang II infusion (Fig. 3C and D). These cellular phenotypes were concordant with a marked suppression of survival signaling

pathways, Akt and Erk1/2 pathways, whereas preventing Ang II-mediated phosphorylation of p38 and JNK1/2 MAPK (*SI Appendix*, Fig. S6). These changes were associated with elevated oxidative stress as evident by the increased number of dihydroethidium (DHE)-positive cells in the aortic wall coupled with elevated NADPH oxidase (Fig. 3E and F and *SI Appendix*, Fig. S5B) and in situ gelatinase activities reflecting the action of matrix metalloproteinases 2 and 9 (*SI Appendix*, Fig. S7).

Next, we characterized the impact of APLN deficiency on VSMCs in response to Ang II in vitro. In cultured primary aortic SMCs from human and mouse aorta (*SI Appendix*, Fig. S8), APLN expression was knocked down using specific APLN-siRNA (siAPLN), whereas scrambled siRNA (siNS) was used as the control (Fig. 4A). Ang II treatment increased *Apln* mRNA levels in control human and mouse SMCs (siNS) but induced a markedly higher rate of apoptotic cell death in the siAPLN SMCs of both species (Fig. 4B) accompanied by elevated oxidative stress and DHE levels in these SMCs (Fig. 4C). ACE2 has emerged as a major negative regulator of the RAS by converting Ang II into Ang 1–7 (5). We identified Ang II-mediated transcriptional up-regulation of *Ace2* mRNA in human and murine VSMCs (Fig. 4D) in association with increased ACE2 protein levels in diseased murine aortas (Fig. 4E and F). Suppression of APLN markedly inhibited Ang II-mediated rise in *Ace2* mRNA and ACE2 levels (Fig. 4D–F). These data demonstrate that Ang II-induced AAA in *Apln*^{-/-} mice is due to the intrinsic susceptibility of the vasculature to adverse remodeling due to the lack

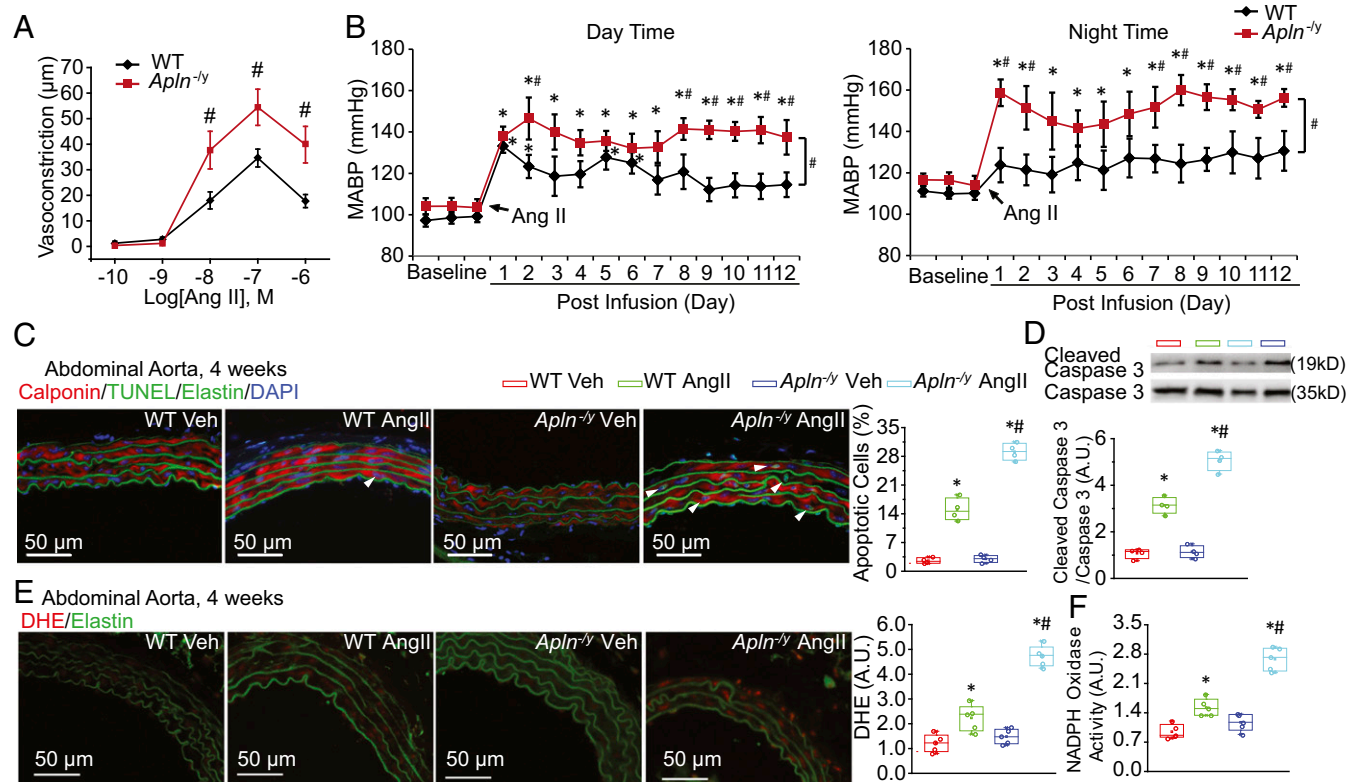


Fig. 3. Loss of APLN sensitizes the vasculature and vascular SMCs to the pathological effects of Ang II using pressure myography and third-order mesenteric arteries in WT and *Apln*^{-/-} vessels; $n = 8/\text{group}$. (B) Telemetry blood pressure recording in WT and *Apln*^{-/-} mice before and over 2 wk of Ang II infusion (1.5 mg/kg/d); MABP; $n = 8/\text{group}$. The arrows indicate when Ang II infusion starts. (C) Immunostaining for SMCs (calponin, red), apoptosis (TUNEL, green), nuclear DAPI staining (blue), and elastin fiber autofluorescence (green) in AA. Averaged percentage of apoptotic cells in each group is shown in the boxes with scatter plots; $n = 4/\text{group/genotype}$. (D) Western blot assay for total and cleaved caspase 3 and averaged cleaved-to-total caspase 3 levels is shown as a box with a scatter plot; $n = 4/\text{group}$. (E) DHE-based fluorescence in the abdominal aortic wall with (F) NADPH oxidase activity ($n = 5/\text{group/genotype}$). * $P < 0.05$ compared with the Veh group; # $P < 0.05$ compared with the WT-Ang II group.

of APLN-mediated up-regulation of ACE2 and its prosurvival effects on VSMCs.

NEP Is a Key Enzyme that Inactivates APLN Peptides. Our results suggest that enhancing APLN action may be a therapeutic strategy for preventing or slowing the progression of AAA, a disease lacking effective medical therapy. We hypothesized that up-regulation of neutral endopeptidase (EC 3.4.24.11, NEP, and neprilysin) (22, 23) in disease degrades endogenous APLN thereby promoting AAA formation. Western blot analysis and immunostaining showed that NEP levels are increased in diseased murine and human aortas (Fig. 5A and B and *SI Appendix, Fig. S9*). We next examined the ability of NEP in inactivating APLN peptides which could provide a fundamental mechanism for the pathogenesis of AAA. Computer modeling and simulation demonstrated a feasible model of APLN-17 binding with the active catalytic site in NEP (His583, His587, and Glu646) resulting in the cleavage of APLN-17 at 2 distinct sites, Arginine8-Lysine9 and Lysine9-Serine10 (Fig. 5C and *SI Appendix, Fig. S10*). Other active site residues in NEP that facilitate the binding of APLN-17 in the catalytic pocket are Arg102, Arg110, Glu533, Val541, Ser546, Ser547, Ile585, Glu646, Ile648, Gly655, Ala657, Tyr697, Val710, His711, and Arg717 (Fig. 5C). To confirm this prediction, we used a biochemical assay and found that ex vivo incubation of APLN-17 in human plasma with recombinant NEP resulted in efficient degradation of APLN whereas the application of a NEP inhibitor, sacubitrilat, elevated steady-state APLN levels (Fig. 6A) with corresponding inverse changes detected in plasma APLN 17 products, APLN 9–17 and APLN 10–17 peptides (*SI*

Appendix, Fig. S11). The APLN degradation products were completely inactive demonstrating a key functional role of NEP in degrading APLN (Fig. 6B). We next tested the in vivo role of NEP in metabolizing APLN-17. Genetic loss or pharmacological inhibition (by sacubitrilat) of NEP potentiated the hypotensive action of APLN-17 (Fig. 6C) and markedly elevated plasma levels of APLN-17 (Fig. 6D). These results highlight a dominant role for NEP in metabolizing and inactivating the endogenous APLN-17 peptide, which implied the NEP resistant APLN analog is much needed for therapeutic use in vivo.

APLN Analogs Have Improve Pharmacokinetics and Equivalent Pharmacodynamics. Native APLN peptides are easily degraded and have short half-lives (14, 24, 25). Therefore, we designed and tested 35 different analogs and were able to identify and develop a long-lasting stable APLN-17 analog NMeLeu9Nle15Aib16BrPhe17-APLN-17 (abbreviated as APLN-NMeLeu9A2) (Fig. 7A) and confirmed a marked improvement in plasma levels and hypotensive effects (Fig. 7B and C). The APLN receptor (formerly known as APJ) is the only known native receptor for APLN peptides in mammals (26). Binding studies with the murine APLN receptor showed that murine Gi activation and β -arrestin recruitment were maintained by APLN-NMeLeu9A2 at similar levels compared with native APLNs, minimizing the possibility of off-target effects of APLN analogs (Fig. 7D–G). Our NEP resistant APLN-17 analog (APLN-NMeLeu9A2) represents a therapeutic approach for AAAs.

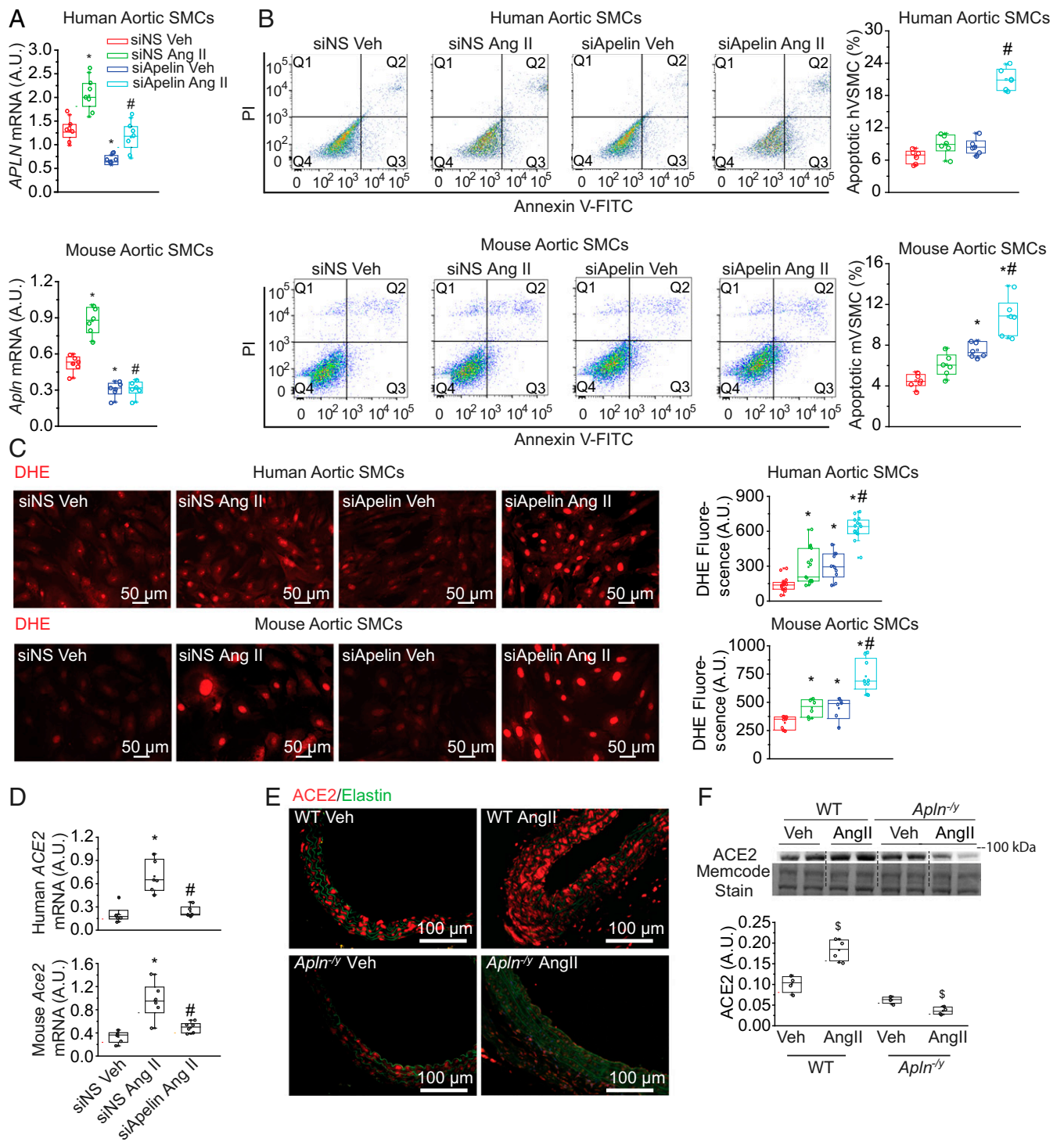


Fig. 4. Down-regulation of APLN expression in murine and human vascular SMCs increases Ang II-mediated cell death and oxidative stress. (A) siRNA treatment reduced *Apln* mRNA levels in human (Upper) and mouse (Lower) cultured primary aortic SMCs. (B) Flow cytometry analysis of cell death in human and mouse SMCs ± siNS or APLN-siRNA (siAPLN) treated with Ang II (10 μM) shows a marked increase in Ang II-induced cell death in APLN-deficient SMCs with quantitative analysis shown in the boxes and scatter plots; *n* = 6/group. (C and D) DHE-based fluorescence from cultured human and murine primary aortic SMCs (C) and *Ace2* mRNA expression (D) in response to siRNA targeting APLN expression (*n* = 6/group/genotype). (E and F) Representative immunostaining for ACE2 (red) and elastin fiber autofluorescence (green) (E) and Western blotting for ACE2 in WT and *Apln*^{-/-} aorta (F) with averaged ACE2 levels shown as a box with a scatter plot; *n* = 4/group. **P* < 0.05 compared with the siNS + Veh group; #*P* < 0.05 compared with the siNS + Ang II group; \$*P* < 0.05 compared with the corresponding Veh group. A.U., arbitrary units.

Therapeutic Effects of a Stable APLN Analog in an Experimental Model of AAA. To test the therapeutic potential of our synthetic APLN analog designed to be resistant to NEP-mediated degradation,

we utilized a well-established model of an AAA. We used a murine model lacking low-density lipoprotein receptors (*Ldlr*^{-/-}) given a HFD and Ang II infusion (21, 27). Although the placebo-treated

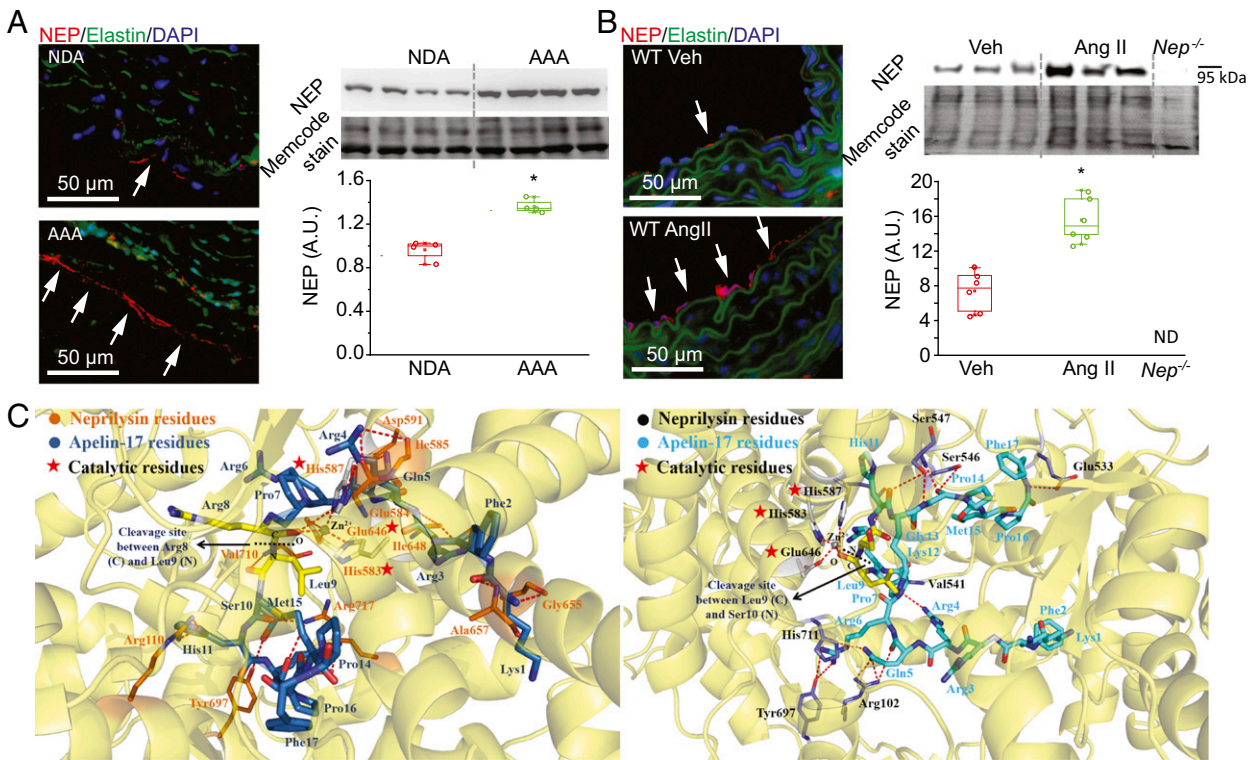


Fig. 5. NEP is up-regulated in the diseased aorta, and computer modeling predicts NEP mediates proteolytic cleavage of APLN-17. (A and B) Immunofluorescence staining and Western blot analysis of NEP in diseased human (A) and murine (B) aorta illustrating increased levels of NEP. *Nep*^{-/-} aorta used as a negative control. ND, not detected; *n* = 4/group in (A), *n* = 6/group in B. (C) Computer-based in silico modeling showing the interaction between the catalytic site of NEP and cleavage sites in native APLN-17 peptide. **P* < 0.05 compared with the NDA or Veh group.

group (*Ldlr*^{-/-}-Ang II + placebo) showed a 50% mortality mainly due to aortic rupture in the abdominal region, treatment with the APLN analog (*Ldlr*^{-/-}-Ang II + APLN-NMeLeu9-A2) had no

incidence of aortic rupture after 4 wk of Ang II infusion (Fig. 8A). Vascular ultrasound showed that the administration of APLN-NMe17A2 prevented aortic lumen dilation and preserved aortic

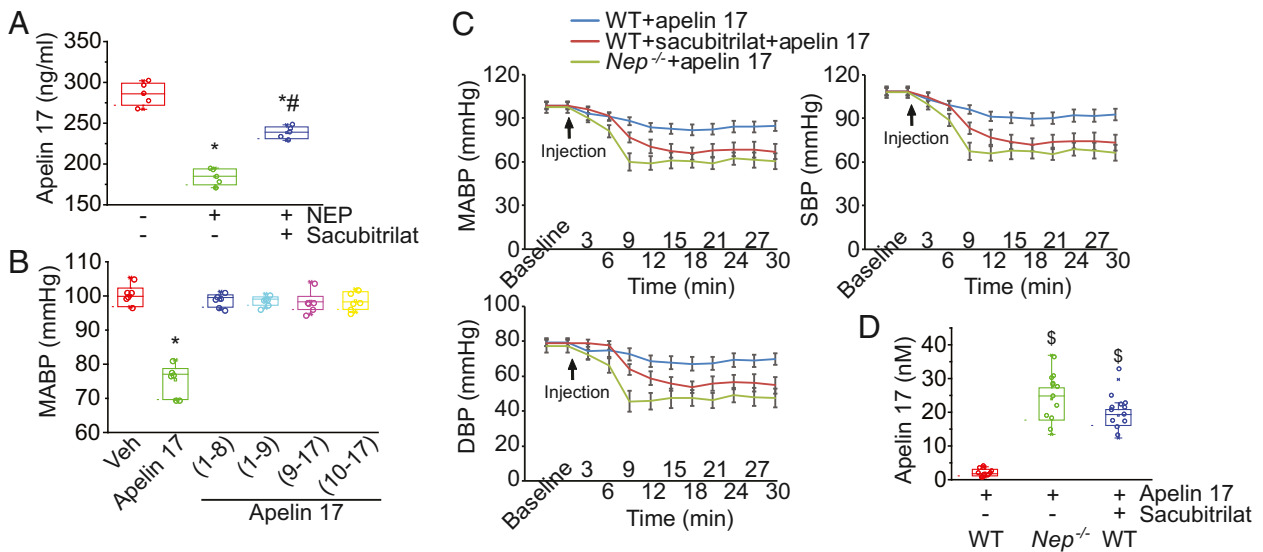


Fig. 6. NEP plays a key role in the inactivation of APLN-17: synthesis of NEP resistant APLN analogs. (A and B) In vitro assay using human plasma and human recombinant NEP demonstrating the ability of NEP to efficiently cleave APLN-17 (A) and in vivo blood pressure assay in WT mice demonstrating that the cleaved products of NEP action on APLN-17 peptides are inactive (B); NEPi = sacubitrilat; *n* = 5 to 6/group. (C) In vivo blood pressure assay in WT mice examining the vasodepressor activity of the NEP-mediated cleavage of the APLN-17 peptide product; *n* = 6/group; Averaged values represent mean ± SEM. MABP; SBP = systolic blood pressure; DBP = diastolic blood pressure. (D) Plasma APLN-17 levels in WT and *Nep*^{-/-} mice and in response to pharmacological inhibition of NEP using sacubitrilat in WT mice; *n* = 12/group. **P* < 0.05 compared with the Veh group; #*P* < 0.05 compared with the NEP group without sacubitrilat; \$*P* < 0.05 compared with the WT group without sacubitrilat.

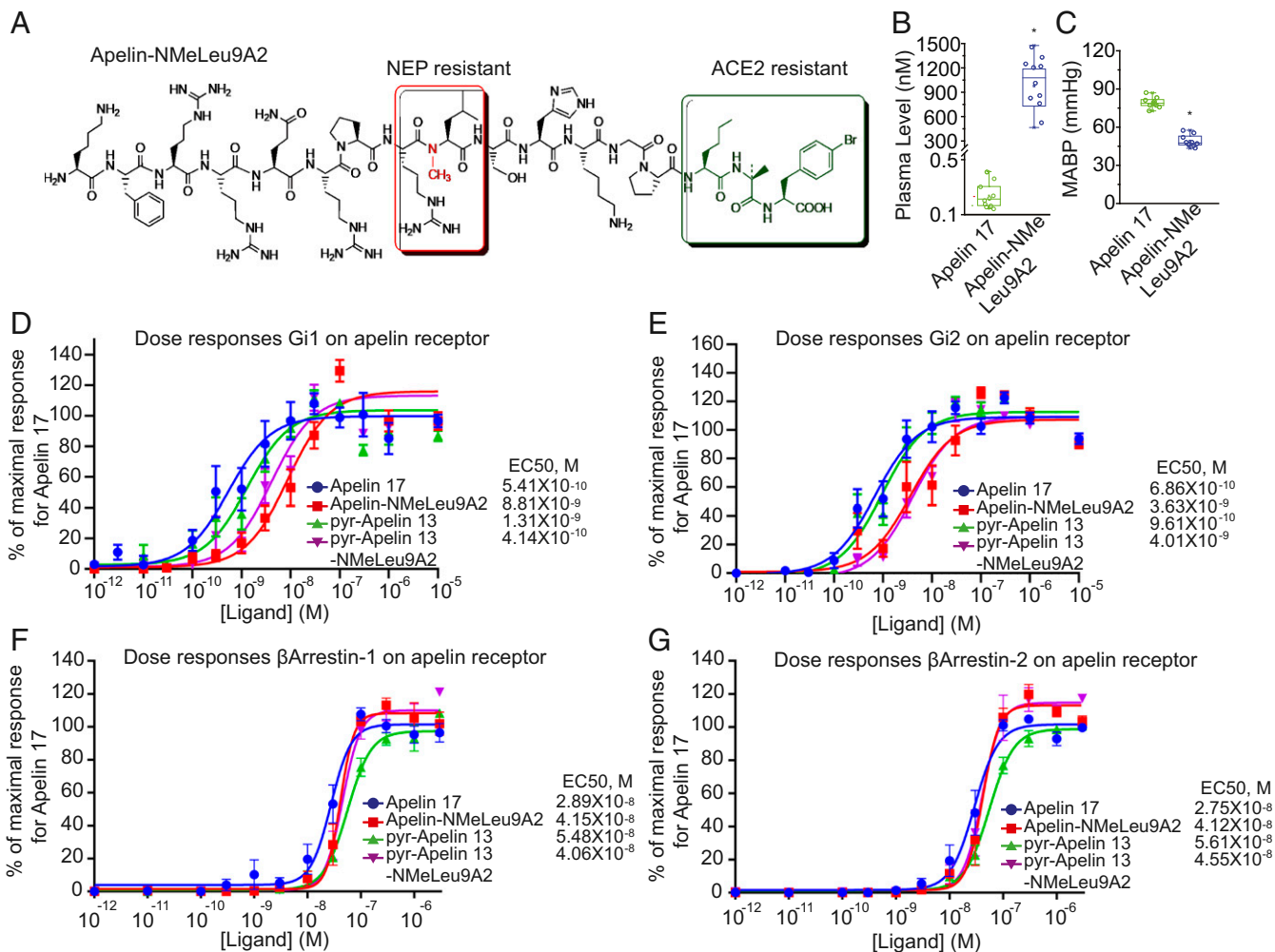


Fig. 7. APLN receptor coupled Gi activation and β -arrestin recruitment by APLN peptides and APLN analogs. (A–C) Schematic of the APLN-NMeLeu9A2 with plasma levels at 5 min post*i.v.* administration and blood pressure response compared with native APLN-17; $n = 10$ /group. * $P < 0.05$ compared with the APLN 17 group. (D–G) Concentration-response effect of endogenous APLN peptides (K17F and pE13F) and metabolically stable APLN analogs (K17FA2 and pE13FA2) on murine (D) Gi1 activation, (E) Gi2 activation, (F) β -arrestin-1 recruitment, and (G) β -arrestin-2 recruitment. The data represent the mean \pm the SEM of 4 to 8 independent experiments performed in duplicate. The data are expressed as percentages of the maximal response obtained for K17F. EC₅₀ are listed on the right side of the concentration-response plots.

compliance (expansion index) (Fig. 8B). Structural analysis of the abdominal aorta provided definitive evidence that Ang II-mediated aortic pathology in *Ldlr*^{-/-} mice was prevented by treatment with APLN-NMe17A2. Importantly, mice receiving APLN-NMeLeu9A2 preserved SMC density and elastin structure, and reduced apoptosis (TUNEL and cleaved caspase 3 levels) in the aortic wall in response to 2 and 4 wk of Ang II infusion (Fig. 8C and D). Intriguingly, APLN analog supplementation increased ACE2 levels in the aortic wall (Fig. 9A and B), which has been reported to have vasculoprotective effects (15). In isolated VSMCs, Ang II-mediated production of reactive oxygen species determined by DHE fluorescence and NADPH oxidase activity were markedly attenuated by APLN-NMe17A2 (Fig. 9C and D). Our results highlighted a dominant role of the APLN pathway in AAA and support the use of a stable APLN analog as a therapy for AAA (Fig. 9E).

Discussion

Vascular diseases remain a major health burden, and AAs lack effective medical therapy representing a progressive disease state with a life-threatening but unpredictable risk for rupture (1, 2). Currently, no pharmacological intervention effectively inhibits

the progressive expansion of human AAAs or prevents aortic rupture (28, 29). In this study, we demonstrate a seminal role for APLN in AAA pathogenesis using loss-of-function and gain-of-function approaches. Using an Ang II-induced model of an AAA, loss of APLN resulted in greater adverse remodeling and propensity to develop an AAA, aortic rupture, and increased mortality. Given the short half-life of native APLN peptides, we identified NEP as a dominant inactivating enzyme for APLN-17. This allowed us to design and synthesize a stable and bioactive APLN analog that is resistant to NEP degradation, active in both blood pressure *in vivo* as well as *in vitro* APLN receptor binding studies; and it showed profound therapeutic effects for AAAs.

In aortic SMCs, APLN showed a dose-dependent protective effect against Ang II-induced apoptosis and reactive oxygen species stress, whereas loss of APLN exacerbated these responses, consistent with a dominant role of apoptotic loss of VSMCs in the progression of AAAs. A well-recognized characteristic in human AAAs is the increased abundance and activation of matrix metalloproteinases in the diseased aortic tissues that was modulated by the APLN pathway likely in response to changes in oxidative stress. APLN action on endothelial cells including promoting angiogenesis (6, 11, 12), APLN-mediated nitric oxide vasodilation

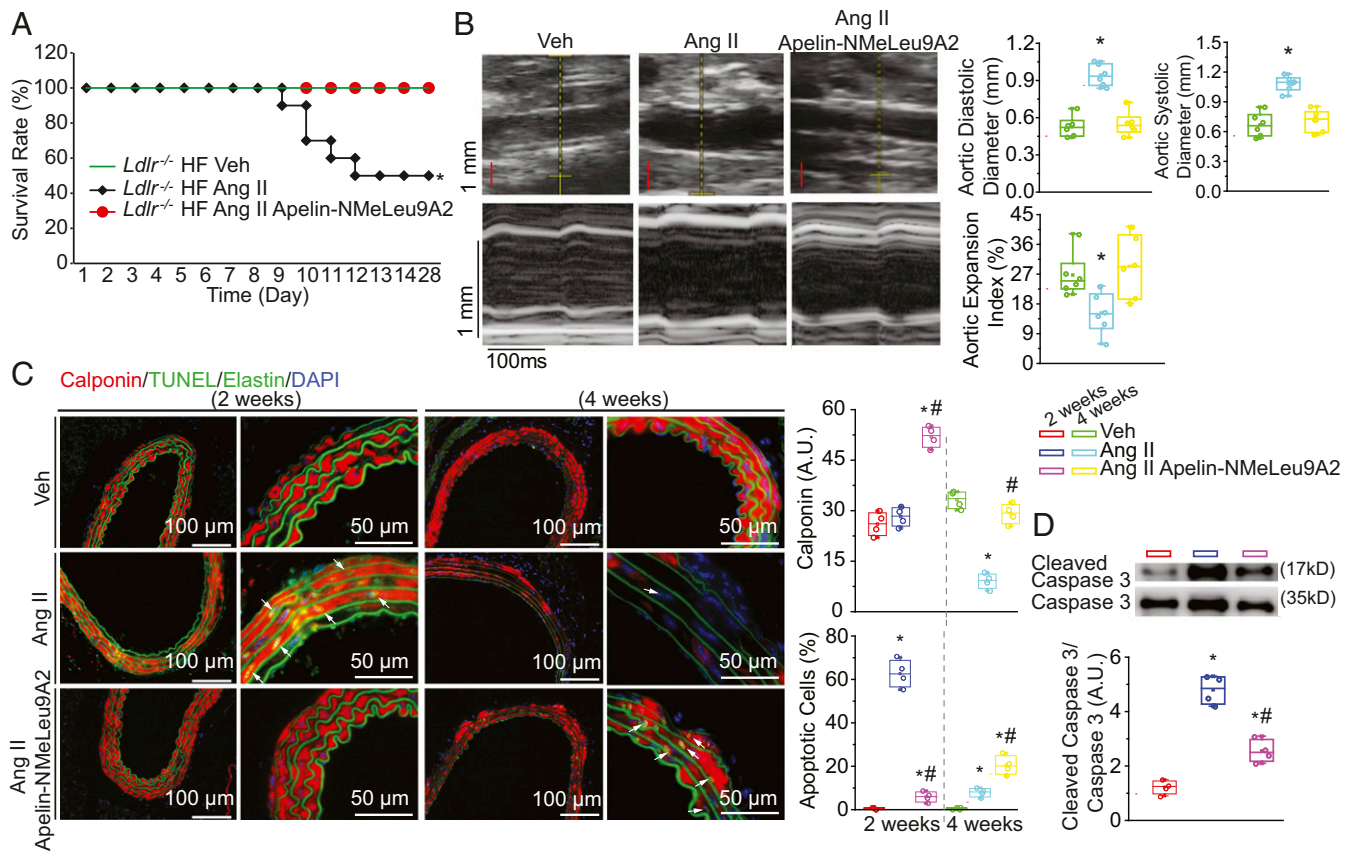


Fig. 8. NEP resistant APLN analog prevents Ang II-induced formation of AAA. (A) Survival curves showing the rate of mortality due to aortic rupture in *Ldlr*^{-/-} mice on a HFD that received Veh (saline) or Ang II for 4 wk (1.5 mg/kg/d), or Ang II + APLN-NMeLeu9A2. Mortality only presented in the HFD-Ang II group and is significantly higher than in other groups; *n* = 15/group. (B) Representative ultrasound images of the AA and averaged measurement for AA diameter during systole and diastole, and aortic expansion index, a measure of aortic wall compliance; *n* = 6/group. (C) Representative images of immunostaining for AA sections for calponin (SMC, red), TUNEL (green), DAPI (blue), and elastin fibers autofluorescence (green) in the indicated groups. Averaged quantification for calponin levels (measure of viable SMCs), and apoptotic cells (TUNEL positive) for each group is shown on the right; *n* = 4/group; arrows point to apoptotic cells. (D) Western blots for cleaved and total caspase 3 and averaged cleaved-to-total ratio for caspase 3; *n* = 4/group. **P* < 0.05 compared with the Veh group; #*P* < 0.05 compared with the Ang II group.

(11), and direct antagonism of the Ang II/Ang II type 1 receptor (10) highlights a key role of endothelial homeostasis as a critical pathway protecting the aorta from AAA formation (29). Ang II increases vascular tone, and excessive activation causes systemic hypertension, which is a major risk factor for AAA, atherosclerosis, and cardiac hypertrophy. The Ang II-induced vasoconstriction was potentiated in *Apln*^{-/-} arteries without affecting passive elasticity and constrictive response to the α -adrenergic agonist PE. Indeed, Ang II-induced greater hypertension in *Apln*^{-/-} mice compared with WT mice; however, this finding also poses a complexity in understanding the role of APLN in Ang II-induced adverse aortic remodeling because of the potential involvement of hypertension. As such, we used a PE-induced hypertension model and cultured murine and human aortic SMCs to demonstrate the specific susceptibility of APLN-deficient VSMCs to the pathological effects of Ang II.

Therapeutic supplementation with our stable APLN analog exhibited protective effects against AAA formation and up-regulated ACE2 which promotes vascular protective remodeling. Indeed, decreased ACE2 in the *Apln*^{-/-} mesenteric artery could contribute to the increased sensibility of these mice to Ang II-induced AAA which highlights the vasculoprotective effect of Ang 1–7 (30). Basal ACE2 levels were lowered in the *Apln*^{-/-} aorta compared with WT and failed to increase in response to Ang II. As such, the Ang II-mediated up-regulation of APLN in WT mice, which, in turn, up-regulates ACE2 leading to the

conversion of Ang II into the protective Ang 1–7 peptide (5, 30) represents a critical negative feedback mechanism to confer vascular protection. The beneficial effects of APLN extend beyond the ACE2 pathway since Ang II infusion in *Ace2*^{-/-} mice does not recapitulate the severe phenotype observed in the *Apln*^{-/-} mice. Indeed, we identified a unique susceptibility of the APLN-deficient VSMCs to Ang II-mediated apoptotic cell death. *Apln*-deficiency reduced Ang II-mediated phosphorylation of Akt and Erk1/2 in the aorta consistent with the ability of the APLN peptide to activate a classic G protein coupled receptor leading to PI3 kinase activation and phosphorylation of Akt and Erk1/2 pathways (6, 14, 31).

Enhancing APLN action offers promising therapeutic effects on the aorta. We show that cleavage of APLN-17 by NEP completely inactivates this peptide, and the marked increase in NEP in a human aorta with AAA is likely a key mechanism of the progression of AAA. Computational modeling of the interaction between NEP and APLN-17 showed that the catalytic residues that promote the cleavage of the peptide, and other active site residues that assist APLN-17 binding are situated in the C-terminal region of the enzyme which implicate a domain specific enzyme catalysis. MICU2, a regulatory subunit of the mitochondrial calcium uniporter complex is protected from Ang II-mediated injury to the abdominal aorta associated with a marked up-regulation of *Apln* expression (20), whereas APLN also mediates protective effects in atherosclerosis (10) consistent

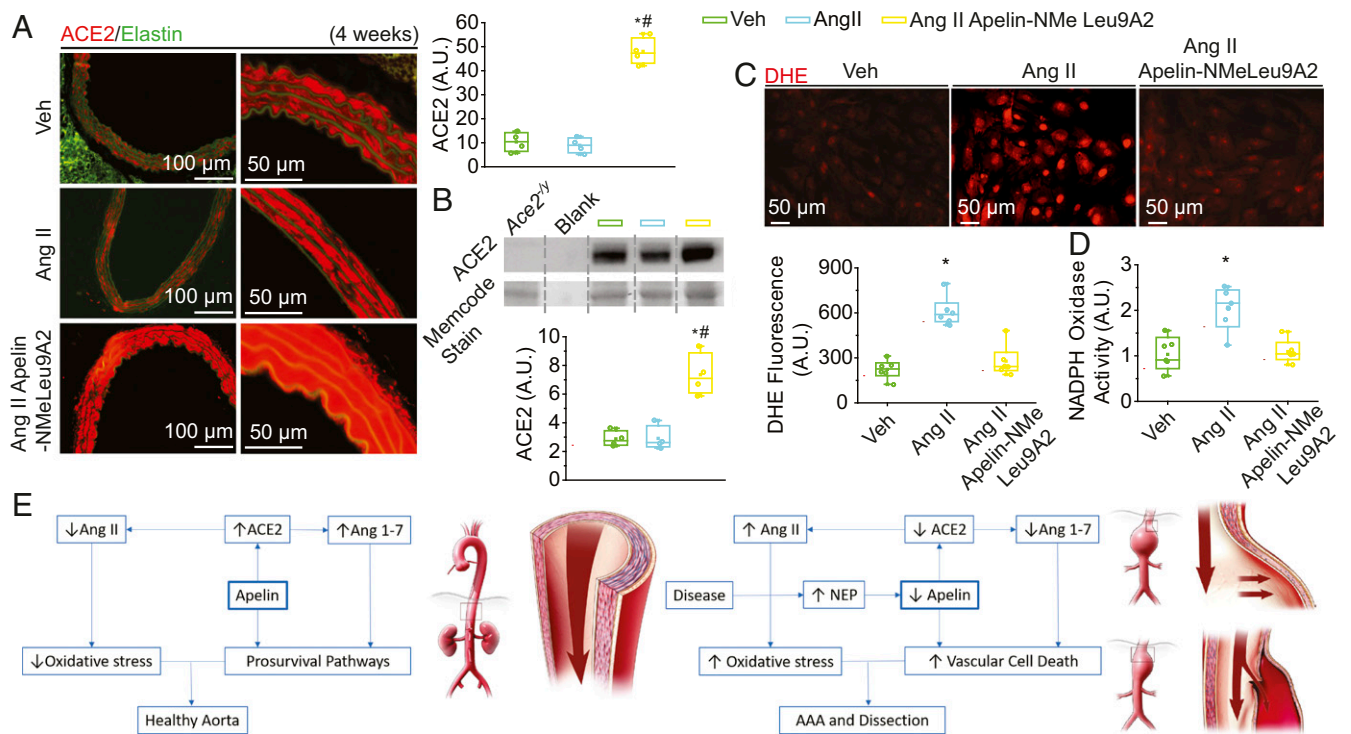


Fig. 9. Up-regulation of ACE2 by APLN analog; role of APLN in AAA pathogenesis. (A) Immunostaining for ACE2 and quantification in the AA of *ldlr*^{-/-} on HFD receiving Veh, Ang II, or Ang II + APLN-NMeLeu9-A2; *n* = 4/group/genotype. (B) Western blots and quantification for ACE2 levels in abdominal aorta of *ldlr*^{-/-} on HFD mice receiving Veh, Ang II + placebo, or Ang II + APLN-NMeLeu9-A2. Aortic proteins from *Ace2*^{+/y} mice were used as a negative control; *n* = 4/group/genotype. (C) DHE-based fluorescence with (D) NADPH oxidase activity in cultured human primary aortic SMCs in response to Ang II and effects of APLN-NMeLeu9-A2; *n* = 6/group. (E) Schematic showing the interaction among APLN, ACE2, and NEP in a pathological setting driving the formation of AAA. **P* < 0.05 compared with the placebo group. A.U., arbitrary units. Averaged values represent mean ± SEM.

with a vascular protective effect of APLN peptides. Our study clearly defines the APLN pathway as a central node in the pathogenesis of AAAs and the therapeutic strategy of enhancing the APLN pathway in treating AA. Enhancing APLN improves metabolic function and prevents sarcopenia and aging-related loss in muscle function (8), protects the failing heart (9, 32, 33) and pulmonary vasculature in patients with pulmonary arterial hypertension (7), and, as such, APLN analogs may confer unique therapeutic effects beyond AAAs.

Materials and Methods

All animal experiments were carried out in accordance with the Canadian Council on Animal Care Guidelines, and animal protocols were reviewed and approved by the Animal Care and Use Committee at the University of Alberta. Diseased and nondiseased human abdominal aortic specimens were collected

at the University of Rochester, NY. Written consent was obtained from all participants, and our study was approved by the University of Rochester, Research Subjects Review Board. Ascending thoracic aorta from patients with bicuspid aortic valve, aortic dilation, and nondiseased aorta were collected as described before (34, 35). Materials and experimental procedures for animal models and protocols, peptide analysis and metabolism, RNA isolation, Taqman PCR, cell culture, tissue and cellular staining and immunofluorescence, flow cytometry, ultrasonic vasculography, vascular myography, blood pressure measurement, computer modeling, receptor binding, protein isolation, Western blotting, and quantification and statistical analysis are described in *SI Appendix, SI Materials and Methods*.

ACKNOWLEDGMENTS. This study was supported by an operating grant from the Canadian Institute for Advanced Research-Molecular Architecture of Life Program (CIHR, Grant 136921) to J.C.V., Canadian Institute for Health Research (CIHR, Grant PJT153306) to Z.K., HSF to G.Y.O. (Grant 855632).

1. K. C. Kent, Clinical practice. Abdominal aortic aneurysms. *N. Engl. J. Med.* **371**, 2101–2108 (2014).
2. X. Li, G. Zhao, J. Zhang, Z. Duan, S. Xin, Prevalence and trends of the abdominal aortic aneurysms epidemic in general population: A meta-analysis. *PLoS One* **8**, e81260 (2013).
3. M. E. Lindsay, H. C. Dietz, Lessons on the pathogenesis of aneurysm from heritable conditions. *Nature* **473**, 308–316 (2011).
4. D. Mozaffarian *et al.*; American Heart Association Statistics Committee and Stroke Statistics Subcommittee, Heart disease and stroke statistics—2015 update: A report from the American heart association. *Circulation* **131**, e29–e322 (2015).
5. V. B. Patel, J. C. Zhong, M. B. Grant, G. Y. Oudit, Role of the ACE2/angiotensin 1-7 axis of the renin-angiotensin system in heart failure. *Circ. Res.* **118**, 1313–1326 (2016).
6. W. Wang *et al.*, Loss of apelin exacerbates myocardial infarction adverse remodeling and ischemia-reperfusion injury: Therapeutic potential of synthetic apelin analogues. *J. Am. Heart Assoc.* **2**, e000249 (2013).
7. L. Brash *et al.*, Short-term hemodynamic effects of Apelin in patients with pulmonary arterial hypertension. *JACC Basic Transl. Sci.* **3**, 176–186 (2018).
8. C. Vinel *et al.*, The exerkine apelin reverses age-associated sarcopenia. *Nat. Med.* **24**, 1360–1371 (2018).

9. M. C. Scimia *et al.*, APJ acts as a dual receptor in cardiac hypertrophy. *Nature* **488**, 394–398 (2012).
10. H. J. Chun *et al.*, Apelin signaling antagonizes Ang II effects in mouse models of atherosclerosis. *J. Clin. Invest.* **118**, 3343–3354 (2008).
11. J. C. Zhong *et al.*, Apelin modulates aortic vascular tone via endothelial nitric oxide synthase phosphorylation pathway in diabetic mice. *Cardiovasc. Res.* **74**, 388–395 (2007).
12. Q. Liu *et al.*, Genetic targeting of sprouting angiogenesis using *Apln*-CreER. *Nat. Commun.* **6**, 6020 (2015).
13. N. De Mota *et al.*, Apelin, a potent diuretic neuropeptide counteracting vasopressin actions through inhibition of vasopressin neuron activity and vasopressin release. *Proc. Natl. Acad. Sci. U.S.A.* **101**, 10464–10469 (2004).
14. S. L. Pitkin, J. J. Maguire, T. I. Bonner, A. P. Davenport, International Union of Basic and Clinical Pharmacology. LXXIV. Apelin receptor nomenclature, distribution, pharmacology, and function. *Pharmacol. Rev.* **62**, 331–342 (2010).
15. V. B. Patel *et al.*, Loss of angiotensin-converting enzyme-2 exacerbates diabetic cardiovascular complications and leads to systolic and vascular dysfunction: A critical role of the angiotensin II/AT1 receptor axis. *Circ. Res.* **110**, 1322–1335 (2012).
16. J. Zhong *et al.*, Angiotensin-converting enzyme 2 suppresses pathological hypertrophy, myocardial fibrosis, and cardiac dysfunction. *Circulation* **122**, 717–728, (2010).

17. M. Haschke *et al.*, Pharmacokinetics and pharmacodynamics of recombinant human angiotensin-converting enzyme 2 in healthy human subjects. *Clin. Pharmacokinet.* **52**, 783–792 (2013).
18. R. Basu *et al.*, Loss of Timp3 gene leads to abdominal aortic aneurysm formation in response to angiotensin II. *J. Biol. Chem.* **287**, 44083–44096 (2012).
19. M. Shen *et al.*, Divergent roles of matrix metalloproteinase 2 in pathogenesis of thoracic aortic aneurysm. *Arterioscler. Thromb. Vasc. Biol.* **35**, 888–898 (2015).
20. A. G. Bick *et al.*, Cardiovascular homeostasis dependence on MICU2, a regulatory subunit of the mitochondrial calcium uniporter. *Proc. Natl. Acad. Sci. U.S.A.* **114**, E9096–E9104 (2017).
21. L. A. Cassis *et al.*, ANG II infusion promotes abdominal aortic aneurysms independent of increased blood pressure in hypercholesterolemic mice. *Am. J. Physiol. Heart Circ. Physiol.* **296**, H1660–H1665 (2009).
22. S. M. McKinnie *et al.*, The metalloprotease neprilysin degrades and inactivates apelin peptides. *Chembiochem* **17**, 1495–1498 (2016).
23. S. M. K. McKinnie *et al.*, Synthetic modification within the “RPRL” region of apelin peptides: Impact on cardiovascular activity and stability to neprilysin and plasma degradation. *J. Med. Chem.* **60**, 6408–6427 (2017).
24. W. Wang *et al.*, Angiotensin-converting enzyme 2 metabolizes and partially inactivates pyr-apelin-13 and apelin-17: Physiological effects in the cardiovascular system. *Hypertension* **68**, 365–377 (2016).
25. C. Fischer *et al.*, Plasma kallikrein cleaves and inactivates apelin-17: Palmitoyl- and PEG-extended apelin-17 analogs as metabolically stable blood pressure-lowering agents. *Eur. J. Med. Chem.* **166**, 119–124 (2019).
26. A. M. O’Carroll, S. J. Lolait, L. E. Harris, G. R. Pope, The apelin receptor APJ: Journey from an orphan to a multifaceted regulator of homeostasis. *J. Endocrinol.* **219**, R13–R35 (2013).
27. C. Bernal-Mizrachi *et al.*, Dexamethasone induction of hypertension and diabetes is PPAR-alpha dependent in LDL receptor-null mice. *Nat. Med.* **9**, 1069–1075 (2003).
28. B. T. Baxter, M. C. Terrin, R. L. Dalman, Medical management of small abdominal aortic aneurysms. *Circulation* **117**, 1883–1889 (2008).
29. M. Shen, M. Hu, P. W. M. Fedak, G. Y. Oudit, Z. Kassiri, Cell-specific functions of ADAM17 regulate the progression of thoracic aortic aneurysm. *Circ. Res.* **123**, 372–388 (2018).
30. R. Basu *et al.*, Roles of angiotensin peptides and recombinant human ACE2 in heart failure. *J. Am. Coll. Cardiol.* **69**, 805–819 (2017).
31. B. Masri, N. Morin, L. Pedebnade, B. Knibiehler, Y. Audigier, The apelin receptor is coupled to Gi1 or Gi2 protein and is differentially desensitized by apelin fragments. *J. Biol. Chem.* **281**, 18317–18326 (2006).
32. Z. Z. Zhang *et al.*, Apelin is a negative regulator of angiotensin II-mediated adverse myocardial remodeling and dysfunction. *Hypertension* **70**, 1165–1175 (2017).
33. A. G. Japp *et al.*, Acute cardiovascular effects of apelin in humans: Potential role in patients with chronic heart failure. *Circulation* **121**, 1818–1827 (2010).
34. J. Lee *et al.*, Gender-dependent aortic remodelling in patients with bicuspid aortic valve-associated thoracic aortic aneurysm. *J. Mol. Med. (Berl.)* **92**, 939–949 (2014).
35. V. B. Patel *et al.*, Angiotensin-converting enzyme 2 is a critical determinant of angiotensin II-induced loss of vascular smooth muscle cells and adverse vascular remodeling. *Hypertension* **64**, 157–164 (2014).

Supplementary Information for

Apelin protects against abdominal aortic aneurysm: therapeutic role of neutral endopeptidase resistant apelin analogues

Wang Wang, Mengcheng Shen, Conrad Fischer, Ratnadeep Basu, Saugata Hazra,
Pierre Couvineau, Manish Paul, Faqi Wang, Sandra Toth, Doran S. Mix,
Marko Poglitsch, Norma P. Gerard, Michel Bouvier, John C. Vederas, Josef M.
Penninger, Zamaneh Kassiri and Gavin Y. Oudit

Correspondence to:

Gavin Y. Oudit, MD, PhD, FRCPC
Email: gavin.oudit@ualberta.ca

This PDF file includes:

SI Materials and Methods

SI References

Table S1

Figures S1 to S11

SI Materials and Methods

Experimental Animals and Protocols. Apelin deficient (*Apln*^{-y}) and littermate wildtype (*Apln*^{+y}) mice were generated and bred in a C57BL/6 background as previously described (1). The *Nep*^{-/-} knockout mice were obtained from Harvard University, which were generated originally as previously described (2) and were backcrossed into C57BL/6 background at least 9 times. Male LDL receptor deficient (*Ldlr*^{-/-}) mice and age-matched wildtype (WT or *Apln*^{+y} or *Ldlr*^{+/+}) mice were generated and bred in a C57BL/6 background. Mice were housed at a constant temperature and humidity with a 12 h–12 h light–dark cycle and free access to food and water. All animal experiments were carried out in accordance with the Canadian Council on Animal Care Guidelines, and animal protocols were reviewed and approved by the Animal Care and Use Committee at the University of Alberta.

Human Explanted Aorta. Diseased and non-diseased human abdominal aortic specimens were collected at the University of Rochester, New York. Written consent was obtained from all participants and our study was approved by the University of Rochester, Research Subjects Review Board. Ascending thoracic aorta from patients with bicuspid aortic valve and aortic dilation, and non-diseased aorta was collected as described before (3, 4).

Angiotensin II (Ang II) and phenylephrine (PE) Infusion in vivo. Alzet micro-osmotic pump (model 1002 or 1004; Durect Co.) was implanted subcutaneously at the dorsum of the neck to deliver Ang II (1.5 mg/kg⁻¹d⁻¹), phenylephrine (PE) (40 mg/kg⁻¹d⁻¹) or vehicle (saline) for 14 days or 28 days in WT, *Apln*^{-y} mice or high-fat fed (42%) *Ldlr*^{-/-} mice (5, 6).

Histological Analyses, TUNEL, and immunofluorescence staining. After 2 weeks or 4 weeks of Ang II or saline infusion, mice underwent whole-body perfusion-fixation via the left ventricle, with

10% buffered formalin (80 mmHg, 20 min). (7) Aortas were dissected and imaged for gross morphological assessment, then fixed in formalin and paraffin-embedded. Three sections were obtained from each aorta and the imaging and analysis were standardized between all groups. Five-micrometer thick formalin fixed paraffin embedded (FFPE) sections of aortas were stained for Movat's pentachrome to evaluate morphological alternations. (7-9) *In situ* DNA fragmentation was detected in 5- μ m thick FFPE aortic sections using the commercially available terminal deoxynucleotidyl transferase-mediated dUTP nick-end labeling (TUNEL) assay kit according to the manufacturer's instructions (Catalog No. A23210, APO-BrdU™ TUNEL Assay Kit, Invitrogen™, Thermo Fisher Scientific Inc. USA) as previously described.(10) Five-micrometer thick FFPE sections were also subjected to immunofluorescent staining for ACE2, calponin, apelin and NEP (7, 10) and detailed below.

Immunostaining for apelin was performed on 5 μ m thick formalin fixed paraffin embedded (FFPE) aortic sections (Ultra Plus®, Thermo Scientific). Sections were treated for 20 mins at 65 °C then deparaffinized and rehydrated stepwise before staining. Antigen retrieval was performed using a citrate buffer. After blocking with 1% bovine serum albumin (BSA), tissue sections were incubated with primary antibodies at 4°C for overnight, goat anti-apelin (Santa Cruz Biotechnology Inc., CA, USA) diluted to 1:100 in 1.5% BSA prepared in phosphate-buffered saline. Secondary antibody of Alexa Fluor 594 conjugated donkey anti-goat (Invitrogen) was used at a dilution of 1:400 and incubated for 1 hr at room temperature. After washing all antibodies, the nuclei were stained using ProLong™ Gold antifade reagent with DAPI (Invitrogen).

Similarly, immunostaining for NEP was performed on 5 μ m thick paraffin-embedded aortic sections (Ultra Plus®, Thermo Scientific). Sections were dried for 20 mins at 65 °C then deparaffinized and rehydrated before staining. Antigen retrieval was performed using a citrate

buffer. After blocking with 1.5% BSA, tissue sections were incubated with mouse NEP antibody (R&D system, AF1126-SP) diluted to 1:100 in 1.5% BSA prepared in phosphate-buffered saline. Secondary antibody of Donkey anti-mouse IgG Alexa Fluor 594 (Invitrogen) was used at a dilution of 1:400 and incubated for 1 hr at room temperature. Following 3 rounds of washing the section, nuclei were stained using ProLongTM Gold antifade reagent with DAPI (Invitrogen). Imaging and quantification for all immune-fluorescent histological staining were performed by MetaMorph[®] Basic (version 7.7.0.0) software. Based on identical imaging conditions among comparing groups, including the exposure time, positive signals were detected and quantified based on pixels and density (reported as arbitrary unit or A.U.) in expressional level studies e.g. calponin, ACE2, apelin and NEP; or manually counted (e.g., TUNEL and DAPI staining) and reported as percentage.

Dihydroethidium (DHE) Staining and NADPH Oxidase Activity. For DHE and NADPH staining, fresh aortas were collected (without perfuse-fixation) and preserved in OCT at -80°C. Nicotinamide adenine dinucleotide phosphate (NADPH) oxidase activity was quantified by lucigenin enhanced chemiluminescence using a single-tube luminometer (Berthold FB12, Berthold Technologies, Germany) modified to maintain the sample temperature at 37°C as previously described. (11) NADPH (1 mM) and Lucigenin (50 µM) were added to 100 µg of protein extracts in the presence or absence of diphenylene iodonium (DPI; 10 µM), a selective inhibitor of flavin-containing enzymes including NADPH oxidase. Light emission was measured every 1 second during a 5-min period using a single-tube luminometer (Berthold FB12, Berthold Technologies, Germany) at 37°C.

Dihydroethidium (DHE) staining was performed on aortic SMCs and OCT-embedded aorta sections and visualized using a fluorescence microscope (Olympus IX81) as previously described.

(11) For SMCs, after 1 hour of incubation with or without Ang II (1 μ M), cells were incubated with DHE (20 μ M DHE, final concentration in culture media; Sigma Aldrich) at 37°C for 30 minutes in the dark. For OCT aorta sections, first thaw slides (Cryosection) to room temperature (RT) for 5min; Cover slides with HBSS 5min; Add DHE solution in HBSS on the sections for 20min RT; then transfer the slides to 37°C for 30min; Wash slides with HBSS 3 times; Add anti-fade-no DAPI on the sections and put on the cover glass. Fluorescence images were captured with a fluorescence microscope (IX81, Olympus) after washing with PBS. Quantitative measurements of DHE fluorescence intensity were carried out using the Metamorph Basic software (version 7.7.0.0), regions congruent to the cell nuclei boundaries were drawn, the average pixel intensities were calculated and corrected by subtracting the background, and reported here as DHE intensity.

Ultrasonic Vasculography. Ultrasonic images of the aortas were obtained in mice anesthetized with 1.5% isoflurane using a Vevo 2100 high resolution-imaging system equipped with a real time microvisualization scan head (RMV 704, Visual Sonics, Toronto, Canada). The operator was blinded to the genotype and treatment of the mice and aortic diameters were measured by M-mode at the ascending thoracic aorta, aortic arch and abdominal aorta. The maximum aortic lumen diameter (corresponding to cardiac systole) and the minimum aortic lumen diameter (corresponding to cardiac diastole) recordings were measured and used to calculate the aortic expansion index [(systolic aortic diameter-diastolic aortic diameter)/systolic diameter \times 100] (7).

Primary Aortic Smooth Muscle Cells (SMCs) Cultures. Primary mouse aortic SMCs were isolated using enzymatic digestion method from 3-4 weeks old male WT and *Apln*^{-y} mice as reported before.(12) Briefly, after removal of the surrounding adipose tissue, aorta was incubated in HBSS

(Catalogue. No. 14025076 Gibco® HBSS, Thermo Fisher Scientific Inc. USA) containing 0.744 U/ml elastase (Catalogue No. LS006365, Worthington Biochemical Corporation, USA), 1 mg/ml collagenase type II (Worthington), and 1 mg/ml trypsin inhibitor (Worthington) for 10 min at 37 °C to facilitate the complete removal of the adventitial layer. The intimal layer was scraped off gently with curved fine-tip forceps after the aorta was opened longitudinally. Then the aorta was minced into small pieces (1 mm×1 mm) and further digested for 2 hours at 37°C. The digestion process was terminated by adding an equal volume of DMEM/F12 culture medium containing 20% FBS (DF20). The cell pellet was collected by centrifugation at 300×g for 5 min, suspended in 1 ml of DF20 and given 48 hrs for attachment and spreading. Primary mouse aortic SMCs were weaned into DMEM/F12 culture medium containing 10% FBS (DF10) after passage 3. Cells at passages 4-7 were used for experiments.

Human primary aortic SMCs were isolated using tissue explant method as before.(13) Tissue specimens from the aortic root of healthy donors were washed twice with sterile ice-cold PBS containing 0.5 µg/ml fungizone (Giboco) and 50 µg/ml gentamycin (Giboco). The endothelial cells were scrapped off from the intimal layer by a sterile scalpel blade. The adventitial layer was removed by curved forceps. The remaining medial layer of the aortic tissue was then gently agitated in HBSS (Giboco). Next, transverse muscle strips (2 mm in width) was peeled off from the medial layers using fine-tip forceps. All the collected muscle strips were cut into smaller cubes (2 mm×2 mm) using a sterile blade. The chopped cubes were then washed twice with HBSS, and evenly distributed into 25 cm² culture flasks with a minimum density of 25 cubes/flask, incubated for 24 hours before an additional 2 ml of DF20 was added. The culture medium was changed every 3 days. After 2weeks, the subconfluent (~70%) cells that migrated from aortic tissue explants were trypsinized and subcultured in DF10. Cells at passages 3-5 were used for experiments. For both primary mouse and

human aortic SMCs, the medium was supplemented with 100 U/mL penicillin and 100 µg/mL streptomycin as the final concentration. The purity of human and mouse aortic SMCs were assessed by staining of two specific SMC markers, smooth muscle myosin heavy chain 11 (MYH 11) and SM22.

Small interfering RNA (siRNA) Transfection. Aortic SMCs were seeded into 6-well plate at a density of 10^5 cells/well (~50% confluency). The cells were transfected with *Apln* siRNA (10 µM) or scrambled siRNA (10 µM) for 48 hours in DF10 in the absence of antibiotics as per the manufacture's instruction (Catalog No. 4392420 and 4390771, Silencer® Select siRNAs, Thermo Fisher Scientific Inc. USA). The efficiency of *Apln* knockdown in *Apln* siRNA treated cells (~97%) was confirmed by Taqman PCR analysis.(14)

Annexin V/Propidium iodide (PI) Staining and Flow Cytometry Analysis. When 90% confluence was reached, *Apln*^{+y}, *Apln*^{-y} and *Apln* siRNA transfected aortic SMCs were serum-starved for 24 hours in DMEM/F12 culture medium containing 0.5% FBS. Cells were then treated with 1 µM Ang II or vehicle for 24 hours. Aortic SMCs exposed to staurosporine (1 µM as the final concentration, Santa Cruz Biotechnology, Inc.) for 6 hours were used as a positive control. Ang II induced apoptosis in aortic SMCs were assessed using an Annexin V-FITC/Propidium iodide (PI) kit for flow cytometry (BD Biosciences) as per manufacturer's instruction. In brief, VSMCs were rinsed with ice-cold PBS and detached using accutase (BD Biosciences). The cells were collected by centrifugation (300-g, 5 min). Cell pellets were further washed twice with ice-cold PBS and resuspended in 100 µl of 1×binding buffer. Five µL of Annexin-V-FITC and 1µl of PI (100 µg/ml) were added to the cells and incubated in dark at room temperature for 15 minutes. After incubation,

400 μ l of binding buffer was added to each sample. Cell apoptosis/death was evaluated using a BD LSR Fortessa and FACSDiva software (BD Biosciences). The acquired data were analyzed with FlowJo software (Treestar, Inc., San Carlos, CA). (15)

***Ex vivo* Mesenteric Artery Pressure Myography.** Mesenteric artery pressure myography was performed using the DMT pressure myography system (Danish Myo Technology (DMT), model P110, Denmark) according to the protocol provided by DMT with modification. Briefly, *Apln*^{+/-y} and *Apln*^{-/-y} mice were anesthetized (2% isoflurane), an intact small segment (~4 mm long) of third order mesenteric artery was isolated and mounted on the pressure myography system. Mounted vessels were pressurized in 10 mmHg increments (from 10 to 60 mmHg), for 5 min per increment. A “wake-up” procedure was performed for all vessels before treatments were introduced which included the following steps: vessel was equilibrated at 60 mmHg, physiological salt solution (PSS) was replaced with 6 mM KPSS (HK) to trigger contraction, vessel was allowed to contract for 3 min, KPSS was washed out with PSS until baseline diameter was reached, KPSS contraction and PSS washes were repeated, and noradrenaline (10^{-6} M) was added to PSS to induce a contraction. Once the contraction of the vessel reached a plateau, acetylcholine (10^{-5} M in the PSS bath) was added to assess endothelium-dependent vasodilation. The vessel was washed 5 times over 30 min, and was then ready for experiments. The volume of the bath was maintained at 10 mL for all treatments. In Ang II dose-response experiments, different amounts of Ang II were added to reach desired final concentration in the bath after the vessel constriction reaches a plateau with the previous dose. In a different set of experiments, to study the vasoconstriction and relaxation of Ang II over time, 0.1 μ M of Ang II was used to induce vasoconstriction for 5 min, then washed with PSS buffer and

vessels were allowed to rest for 30 min. For the second treatment, 0.1 μM of Ang II was used to induce vasoconstriction for another 5 min and vessel diameter was continuously recorded.

Continuous Blood Pressure Recording in Conscious Mice. The *Apln*^{+/-} and *Apln*^{-/-} mice were individually housed at a constant temperature ($21\pm 1^\circ\text{C}$) and relative humidity ($50\pm 2\%$) to give them sufficient cage space and avoid signal interference. DSI PhysioTel PA-C10 Pressure Transmitter (Data Sciences International, St. Paul, MN) was implanted subcutaneously in the abdominal region and the catheter cannulated into the aorta via the right carotid artery.⁽¹⁶⁾ Mice were allowed to recover from surgery for one week, after which baseline blood pressure was recorded for 3 days. The sampling hours for blood pressure on each day were 12am to 2am (night) and 12pm to 2pm (day). Subsequently, Ang II (1.5mg/kg/d) was delivered by micro-osmotic pump implanted subcutaneously in the dorsum of the neck. Blood pressure was recorded each day for 12 days after Ang II pump implantation.

Apelins and Analogues Intravenous Injection, Blood Pressure Measurement. The *Apln*^{+/-} and *Nep*^{-/-} mice were anesthetized using 1.5% isoflurane/oxygen, and body temperature was monitored and maintained at 37°C . The aortic arch was reached via the right carotid artery using a PV loop catheter (Model 1.2F from Scisense, Transonic) in order to record arterial blood pressure and heart rate. Data was recorded and analyzed with software LabScribe 2.0, Scisense. Apelin 17 (1.4 $\mu\text{mole/kg}$, Tocris Bioscience, Bristol, UK), or apelin 17 fragments (1-8), (1-9), (9-17) or (10-17) (1.4 $\mu\text{mole/kg}$ body weight) or apelin analogue (Apelin-NMe 17 A2, 1.4 $\mu\text{mole/kg}$ body weight) or same volume of vehicle were given via the right jugular vein. For Nephylin inhibition, Sacubitrilat (1.3 mmole/kg body weight i.v.) was given 10 min in advance. Blood pressure was recorded as baseline for 5 mins after stabilization and for 30 mins after giving drugs.

Western Blot and Taqman PCR analyses. Protein was extracted from aorta using RIPA lysis buffer containing protease and phosphatase inhibitor cocktails, and quantified using the BCA Protein Array Kit (Pierce, Rockford, IL). Equal amounts of protein extracts were loaded and separated by SDS-PAGE gel and then transferred to polyvinylidene fluoride (PVDF) membranes. The membranes were blocked for 1 hr at room temperature with 5% skim milk in TBST, and then incubated with primary antibodies overnight at 4°C, followed by HRP-linked secondary antibodies. The probed proteins were detected with Amersham ECL Prime detection reagent and visualized with ImageQuant LAS 4000 Mini Biomolecular Imager (GE Healthcare, Baie-d'Urfé, QC, Canada). The expression levels of target proteins were quantified by densitometry using the equipped software and reported as ratio over loading control and reported as arbitrary unit (A.U.). Primary antibodies used in this study were: ACE2 (ab15348, Abcam), APLN (ab59469, Abcam), and NEP (AF1126-SP, R&D system). Equal loading of protein was confirmed by staining the membrane with Pierce™ Reversible Protein Stain Kit for PVDF Membranes (ThermoFisher Scientific, USA). *Apln* mRNA expression in aortic SMCs was quantified by Taqman analysis as previously described (17).

Modeling of Apelin-17 Interaction with NEP. We selected the structure of human neprilysin complex with sacubitrilat, an ethyl ester prodrug of LBQ657 (PDB ID: 5JMY), because of its high quality resolution (2Å), appropriate R-factor (free: 0.228, work: 0.186), and errorless electron density map for the preparation of apelin-17 bound neprilysin complex model(18). This structure was then equilibrated in constant pressure-temperature condition (NVT, NPT) in the Groningen Machine for Chemical Simulations (GROMACS). We performed a knowledge-based docking using the binding grid of the ligand sacubitrilat obtained from the above mentioned bound complex

structure of human neprilysin. We built the structure of peptide apelin 17 using the modelling server Peptide Builder (<http://www.peptidesguide.com/peptide-builder.html>). We used the Autodock Vina docking method to model the neprilysin-apelin 17 complexes (19). The grid for docking was developed using structurally aligned sacubitrilat with apelin-17. Using the built-in Grid map option, we prepared the axes dimensions and centre points for performing the docking of apelin 17 with human neprilysin. After selecting the conformations of the ligand that best fit with the conformation of bound sacubitrilat in reference template of human neprilysin, we refined and optimized the complex based on the active site residues using COOT (20). For visualization, analysis of the structural features, detecting peptide interactions and catalytic residues involved in peptide hydrolysis, we used PyMol(21) and Chimera (22).

Measurement of Plasma Apelin Peptide and Analogue. Circulating apelin peptide concentrations were determined by mass spectrometry (MS) using plasma samples collected in the presence of an inhibitor cocktail completely blocking peptide metabolism, containing broad spectrum inhibitors against metalloproteases (EDTA, 1,10-phenanthroline), aspartic proteases (pepstatin A), cysteine proteases (p-hydroxymercuribenzoic acid), serine proteases (AEBSF), and specific inhibitors for renin and aminopeptidases A and N to a final concentration of 5% v/v (Attoquant Diagnostics, Vienna, Austria). (23)

Plasma Apelin Measurement. Stabilized protease inhibitor (see above) plasma was spiked with 200 pg of stable isotope-labelled internal standards of apelin 17 (Sigma Aldrich) and subjected to C18-based solid phase peptide extraction and subsequent LC-MS/MS analysis using a reversed phase analytical column operating in line with a Xevo TQ-S and the apelin analogue, Apelin-

NMeLeu9A2. Stable isotope labelled apelin 17 was used as internal standard for apelin 17. Apelin and analogue concentrations were calculated considering the corresponding response factors determined in calibration curves in original sample matrix, on condition that integrated signals exceeded a signal to-noise ratio of 10.

Apelin 17 Metabolism in Human Plasma. Metabolic analysis of apelin 17 was investigated in human plasma in the presence of recombinant human NEP. A solution of 1 µg/ml of apelin 17 was spiked with plasma of healthy volunteers supplemented with 100 ng/ml recombinant human NEP (Catalogue No. 10805-HNCH, Sino Biological, Canada) and incubated at 37 °C for 0, 5, 10 and 20 min. Following incubation periods, samples were spiked with 200 pg of stable isotope labelled internal standards for apelin 17 (Sigma-Aldrich) and subjected to solid-phase-extraction and subsequent LC-MS/MS-analysis. Calibration curves for the apelin metabolites, apelin 9-17 and apelin 10-17 (Life Tech Austria), were prepared in the original sample matrix. The role of recombinant human NEP in metabolizing apelin 17 was investigated in human plasma with and without the NEP inhibitor, sacubitrilat. A solution of 1 µg/ml of apelin 17 was spiked to plasma of healthy volunteers in presence and absence of 100 ng/ml recombinant human NEP (Sigma-Aldrich) and in the presence or absence of the NEP-inhibitor, sacubitrilat (10 µM, Sigma-Aldrich) and incubated at 37 °C for 20 min. Following incubation, samples were spiked with 200 pg of isotope labelled internal standards for apelin 17 (Sigma-Aldrich) and subjected to solid-phase-extraction and LC-MS/MS-analysis as described above.

Apelin and Analogue Receptor Binding Study. The mouse apelin receptor (formerly APJ) plasmid was purchased from Origene (Rockville, MD, USA). The pE13F and K17F peptides were

purchased from Abcam (Toronto, ON, Canada). The Gibson assembly kit was purchased from New England Biolabs (Ipswich, NE, USA).

Cloning: The mouse apelin receptor plasmid was subcloned from pCMV6 to pcDNA3.1 using the Gibson assembly kit and the NheI and EcoRI restriction sites. The primer was designed as follow:

Primer Forward 5'-

CTCACTATAGGGAGACCCAAGCTGGCTAGCGGATCCGGTACCGAGGAGATCT-3' and

Primer Reverse 5'-

GGCCGCCACTGTGCTGGATATCTGCAGAATTCAGTCCACAAGGGTTTCTTGACTATAG
GG-3'.

Cell Culture and Transfection: All reagents and cell culture supplies, except where specified, were obtained from Invitrogen (Carlsbad, CA, USA). HEK293T cells were cultured in DMEM supplemented with 10% new calf serum and 100 U/mL penicillin/streptomycin at 37 °C under 5% CO₂. Cells were seeded in 150cm² flasks (Corning, Corning, NY, USA) and 48 hours before the experiments, transiently transfected with the mouse apelin receptor in combination with BRET-based biosensor cDNAs. Transient transfections were performed using 25 kDa linear polyethylenimine (PEI – Polysciences, Warrington, PA, USA) at a ratio of 3:1 PEI/DNA. The total amount of transfected DNA was kept constant (100 ng/wells) by the addition of salmon sperm DNA.

BRET measurements for murine Gi activation and β -arrestin recruitment: Gi1 and Gi2 activation were assessed using BRET-based biosensors composed of *Gai1*-RlucII (24) or *Gai2*-RlucII (25) co-expressed with G β 1 and G γ 1-GFP10. β -arrestin recruitment was assessed by monitoring ebBRET between β -arr1-RLucII or β -arr2-RLucII rGFP-CAAX (26). Forty-eight hours following transfection with the appropriate biosensors and apelin receptor, cells were stimulated with the

ligands for 1 or 5 min for the evaluation of Gi activation and β -arrestin recruitment, respectively. The luciferase substrate, coelenterazine 400a (2.5 μ M) was added 5 min before the reads. BRET was monitored with a Mithras LB 940 (Berthold Technologies, Bad Wildbad, Germany) equipped with a 410/70-nm donor filter and a 515/20-nm acceptor filter. The data were analyzed in Prism (GraphPad) using ‘dose-response-stimulation log(agonist) vs normalized response-variable slope’ with the constraint of sharing the Hill slope across all dataset.

Apelin Analogue and Aortic Aneurysm. Male *Ldlr*^{-/-} mice (The Jackson Laboratory) received high fat diet (21% fat by weight, 42% kcal from fat, Teklad, Envigo TD.88137) at 8 weeks of age and throughout the study. One week after initiating high fat diet, osmotic pumps (Model 1004, Alzet) were implanted subcutaneously to deliver angiotensin II (Sigma-Aldrich) at a rate of 1.5 mg/kg/d for 28 days. Synthesized apelin analogue (Apelin-NMeLeu9A2) was given by daily intraperitoneal injection (3 mg/kg/d) for 28 days.

Statistical Analysis. Statistical analyses were performed using SPSS software (Chicago, IL; Version 19). Hypothesis testing methods included Student’s t test or one-way analysis of variance followed by the Student Neuman-Keuls or Tukey. Survival data was analyzed using the Kaplan-Meier method and the log-rank test was used to test for statistical significance. Statistical significance is recognized at $p < 0.05$. Quantitative data are shown as box and scatter plots. The sample size throughout the manuscript indicates the number of independent samples.

SI References

1. Kuba K, *et al.* (2007) Impaired heart contractility in Apelin gene-deficient mice associated with aging and pressure overload. *Circ Res* 101(4):e32-42.
2. Lu B, *et al.* (1997) The control of microvascular permeability and blood pressure by neutral endopeptidase. *Nature medicine* 3(8):904-907.
3. Lee J, *et al.* (2014) Gender-dependent aortic remodelling in patients with bicuspid aortic valve-associated thoracic aortic aneurysm. *Journal of molecular medicine* 92(9):939-949.
4. Patel VB, *et al.* (2014) Angiotensin-converting enzyme 2 is a critical determinant of angiotensin II-induced loss of vascular smooth muscle cells and adverse vascular remodeling. *Hypertension* 64(1):157-164.
5. Zhong J, *et al.* (2010) Angiotensin-converting enzyme 2 suppresses pathological hypertrophy, myocardial fibrosis, and cardiac dysfunction. *Circulation* 122(7):717-728, 718 p following 728.
6. Zhong J, *et al.* (2011) Prevention of angiotensin II-mediated renal oxidative stress, inflammation, and fibrosis by angiotensin-converting enzyme 2. *Hypertension* 57(2):314-322.
7. Basu R, *et al.* (2012) Loss of Timp3 gene leads to abdominal aortic aneurysm formation in response to angiotensin II. *The Journal of biological chemistry* 287(53):44083-44096.
8. Shen M, *et al.* (2015) Divergent roles of matrix metalloproteinase 2 in pathogenesis of thoracic aortic aneurysm. *Arteriosclerosis, thrombosis, and vascular biology* 35(4):888-898.
9. Basu R, *et al.* (2013) TIMP3 is the primary TIMP to regulate agonist-induced vascular remodelling and hypertension. *Cardiovascular research* 98(3):360-371.
10. Patel VB, *et al.* (2012) Loss of angiotensin-converting enzyme-2 exacerbates diabetic cardiovascular complications and leads to systolic and vascular dysfunction: a critical role of the angiotensin II/AT1 receptor axis. *Circulation research* 110(10):1322-1335.
11. Patel VB, *et al.* (2012) Cardioprotective effects mediated by angiotensin II type 1 receptor blockade and enhancing angiotensin 1-7 in experimental heart failure in angiotensin-converting enzyme 2-null mice. *Hypertension* 59(6):1195-1203.
12. Metz RP, Patterson JL, & Wilson E (2012) Vascular smooth muscle cells: isolation, culture, and characterization. *Methods in molecular biology* 843:169-176.
13. Proudfoot D & Shanahan C (2012) Human vascular smooth muscle cell culture. *Methods in molecular biology* 806:251-263.
14. Kasai A, *et al.* (2013) Inhibition of apelin expression switches endothelial cells from proliferative to mature state in pathological retinal angiogenesis. *Angiogenesis* 16(3):723-734.
15. Rieger AM, Nelson KL, Konowalchuk JD, & Barreda DR (2011) Modified annexin V/propidium iodide apoptosis assay for accurate assessment of cell death. *J Vis Exp* (50).
16. Shen M, Morton J, Davidge ST, & Kassiri Z (2017) Loss of smooth muscle cell disintegrin and metalloproteinase 17 transiently suppresses angiotensin II-induced hypertension and end-organ damage. *Journal of molecular and cellular cardiology* 103:11-21.
17. Wang W, *et al.* (2013) Loss of Apelin exacerbates myocardial infarction adverse remodeling and ischemia-reperfusion injury: therapeutic potential of synthetic Apelin analogues. *Journal of the American Heart Association* 2(4):e000249.

18. Schiering N, *et al.* (2016) Structure of neprilysin in complex with the active metabolite of sacubitril. *Scientific reports* 6:27909.
19. Trott O & Olson AJ (2010) AutoDock Vina: improving the speed and accuracy of docking with a new scoring function, efficient optimization, and multithreading. *Journal of computational chemistry* 31(2):455-461.
20. Emsley P & Cowtan K (2004) Coot: model-building tools for molecular graphics. *Acta crystallographica. Section D, Biological crystallography* 60(Pt 12 Pt 1):2126-2132.
21. DeLano WL (2002) The PyMOL molecular graphics system. San Carlos, CA: DeLano Scientific. Retrieved from <http://www.pymol.org>.
22. Pettersen EF, *et al.* (2004) UCSF Chimera--a visualization system for exploratory research and analysis. *Journal of computational chemistry* 25(13):1605-1612.
23. Basu R, *et al.* (2017) Roles of Angiotensin Peptides and Recombinant Human ACE2 in Heart Failure. *J Am Coll Cardiol.* 69 (7):805-819.
24. Gales C, *et al.* (2006) Probing the activation-promoted structural rearrangements in preassembled receptor-G protein complexes. *Nature structural & molecular biology* 13(9):778-786.
25. Quoyer J, *et al.* (2013) Pepducin targeting the C-X-C chemokine receptor type 4 acts as a biased agonist favoring activation of the inhibitory G protein. *Proceedings of the National Academy of Sciences of the United States of America* 110(52):E5088-5097.
26. Namkung Y, *et al.* (2016) Monitoring G protein-coupled receptor and beta-arrestin trafficking in live cells using enhanced bystander BRET. *Nature communications* 7:12178.

Table S1. Subject Demographics

	AAA	NDA	p-value
N=	7	5	
Cadaver (%)	23	100	<0.01
Age (Years)	72±9	73±11	0.89
Male (%)	71	60	
Size (cm)	6.7±2.0	2.0±0.2	<0.01
DM (%)	29	40	0.68
HTN (%)	71	50	0.43
CKD (%)	29	20	0.74
COPD (%)	29	0	0.19
Afib (%)	14	20	0.79
Current Smoker (%)	86	60	0.31
Statin (%)	57	40	0.56
ACE-Inhibitor (%)	14	40	0.31
Beta-Blocker (%)	80	60	0.49
Anticoagulation (%)	14	0	0.38
ASA (%)	71	50	0.43

AAA = Abdominal Aortic Aneurysm

NDA = Non-diseased Aorta

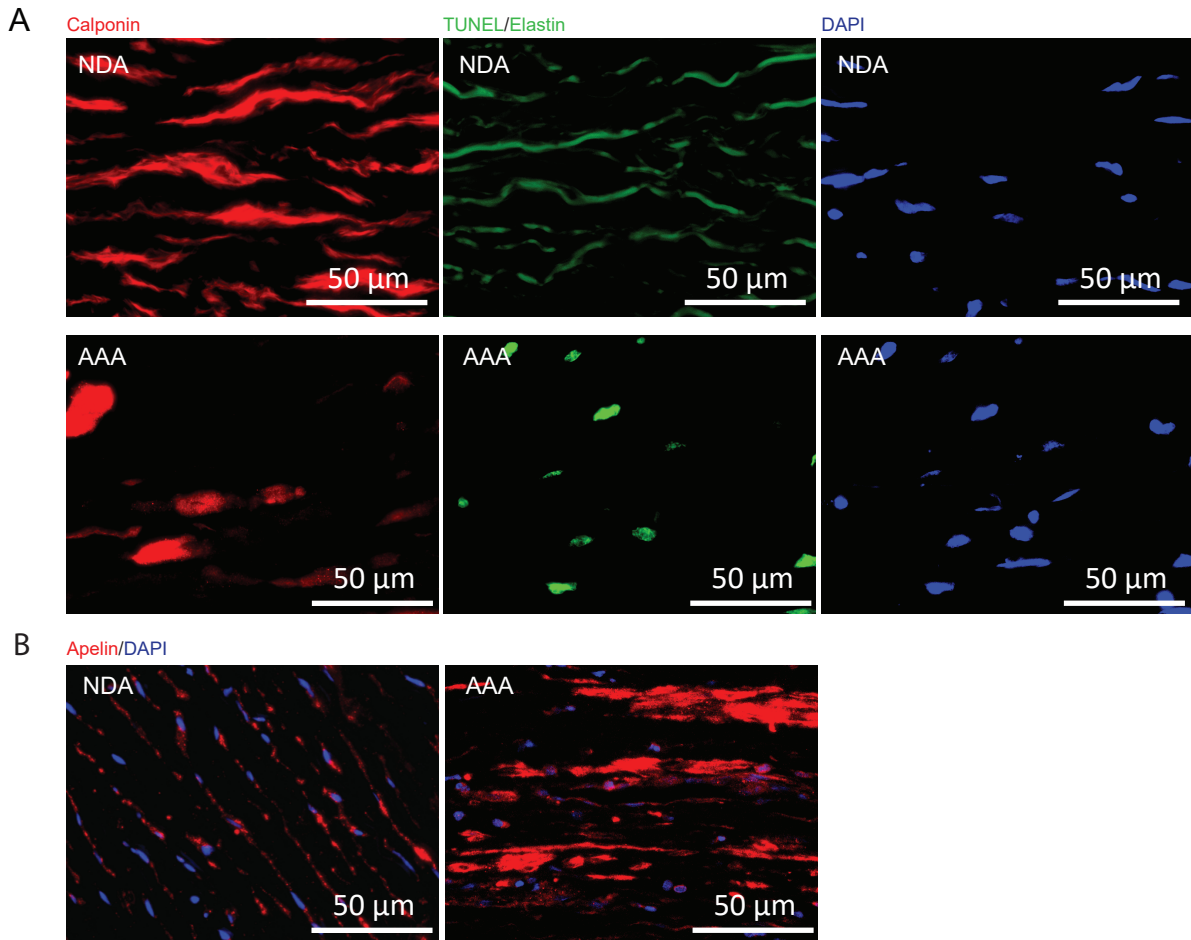


Figure S1. Larger magnification images of the immunohistological staining of abdominal aortic specimens. (A) Surgical resected abdominal aortic aneurysm (AAA) specimens from patients stained with calponin to visualize smooth muscle cells (red). NDA=non-diseased aorta; Elastin fiber autofluorescence appears green; DAPI staining (blue) was used to visualize the nuclei. (B) Immunostaining for apelin (red) showing increased apelin levels in an AAA specimen compared to NDA.

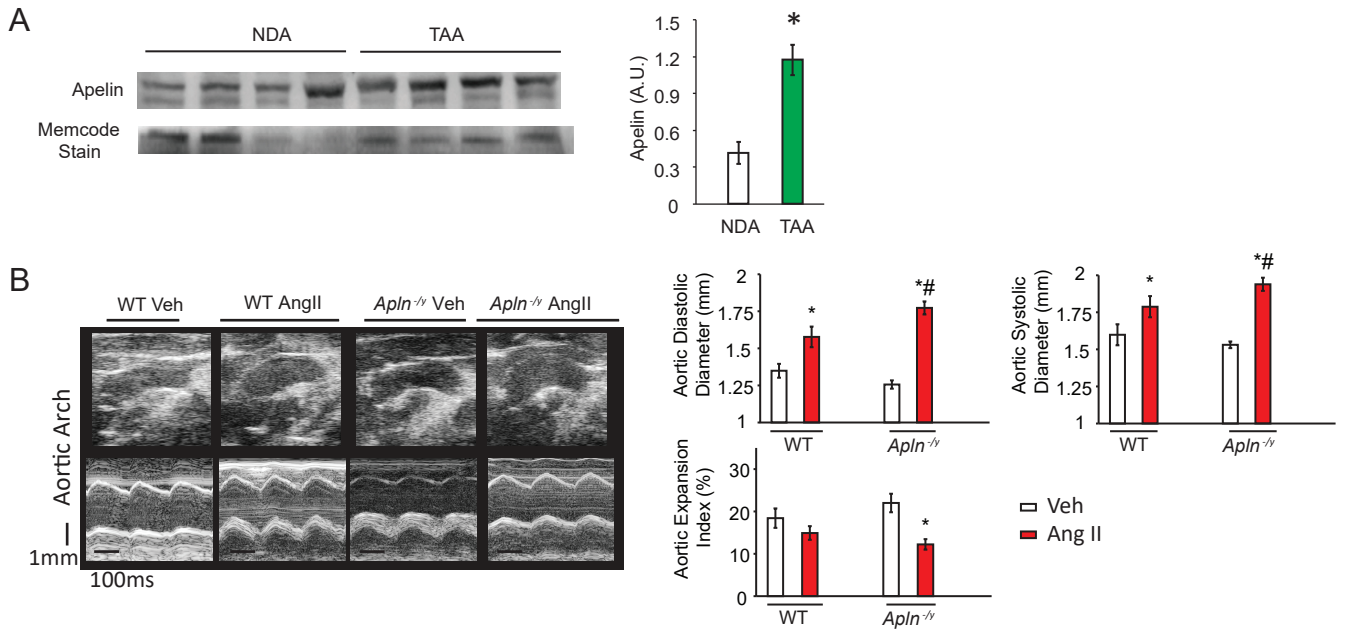


Figure S2. Adverse remodeling in the thoracic aorta in response to Ang II. (A) Western blot analysis for apelin in human thoracic (ascending) aneurysmal aorta (TAA) compared to non-diseased thoracic aorta (NDA); n=4 for each group. (B) Age-matched WT and *Apln*^{-/-} mice show no difference in aortic lumen diameters at baseline (vehicle) but with a greater increase in aortic lumen diameter in the aortic arch in *Apln*^{-/-} compared to wildtype (WT) mice in response to Ang II. Veh=saline; Ang II=angiotensin II. *p<0.05; n=12 for WT, n=18 for *Apln*^{-/-}.

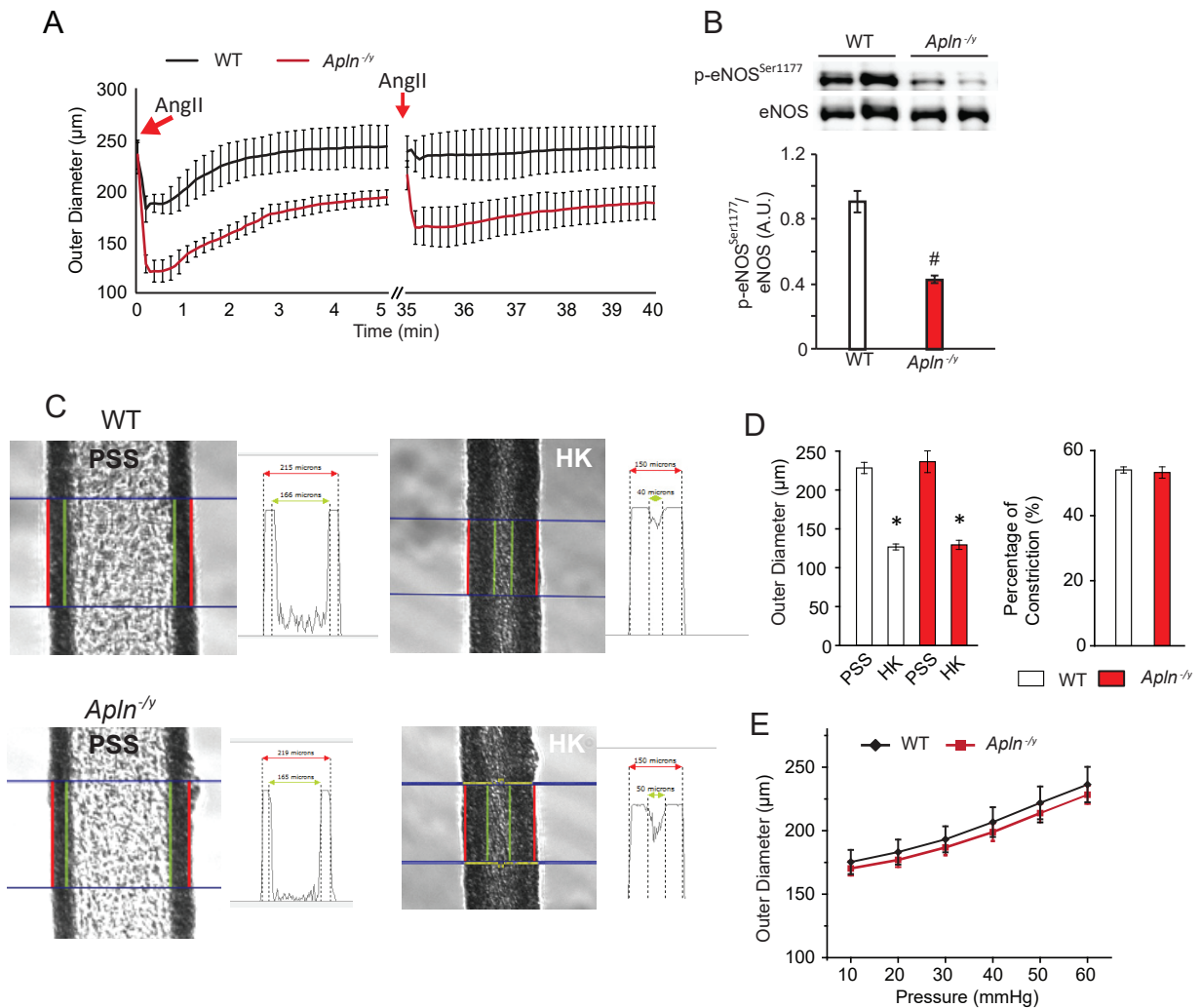


Figure S3. Loss of apelin leads to greater mesenteric artery vasoconstriction in response to Ang II without affecting intrinsic myogenic response. (A) *Apln*^{-/-} mesenteric artery demonstrated greater extent and more sustainable constriction in response to Ang II treatment, as well as maintained responsiveness on repeated Ang II stimulation; n=8 per group. (B) Western blot assay of p-eNOS^(Ser1177) and eNOS levels in WT and *Apln*^{-/-} aorta revealed a marked decrease in p-eNOS^(Ser1177) levels in *Apln*^{-/-} aorta; n=4 per group. (C) Representative images of mesenteric arteries in PSS and HK treatment with WT and *Apln*^{-/-} mesenteric arteries showing similar lumen and outer diameter under PSS, and comparable maximal constriction induced by HK treatment (D); n=8 per group. (E) WT and *Apln*^{-/-} mesenteric arteries showed similar passive elasticity in PSS, tested using pressure myography. PSS: physiological salt solution; HK: high potassium solution. *p<0.01 compare to PSS group; #p<0.01 compare to WT group.

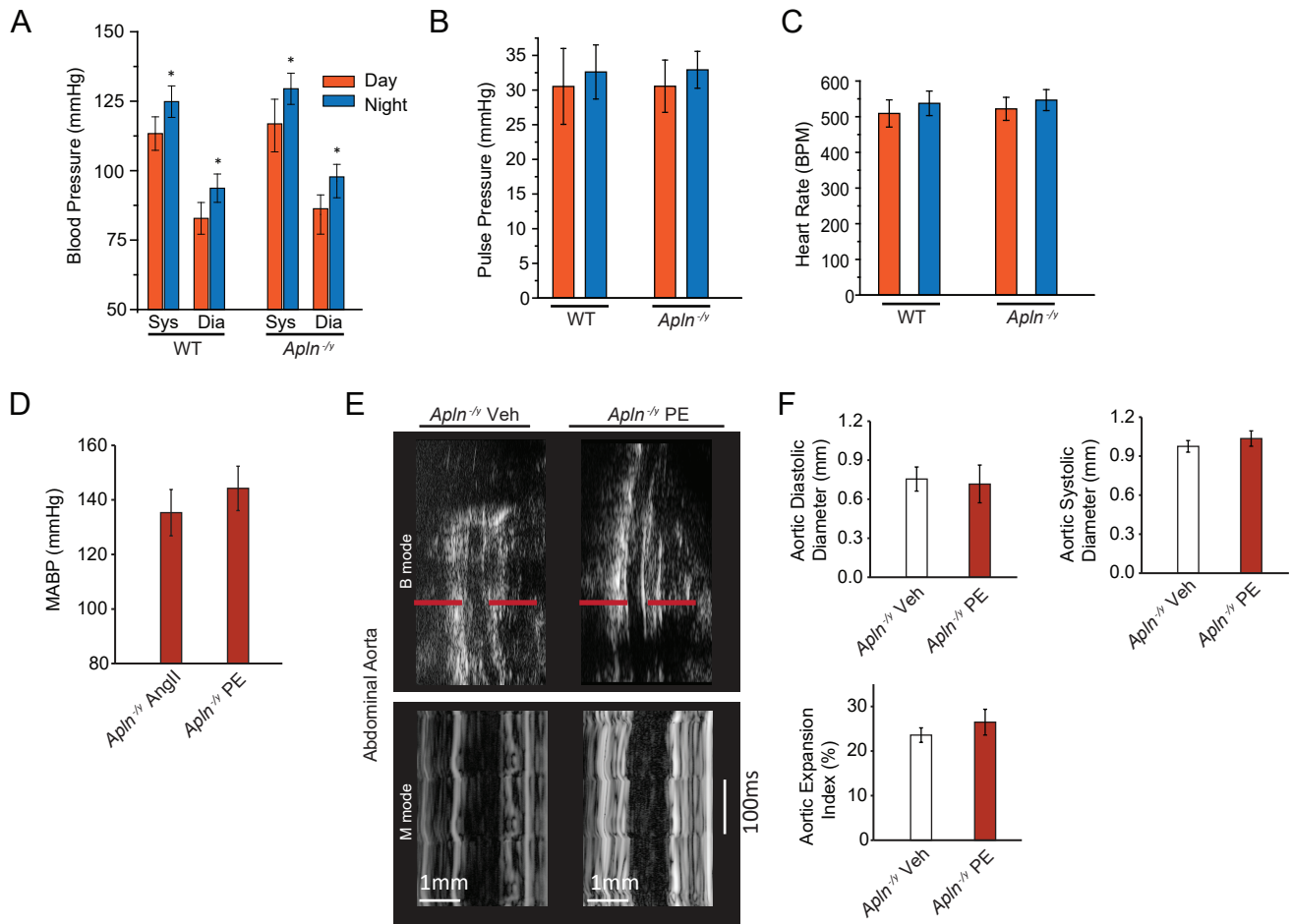
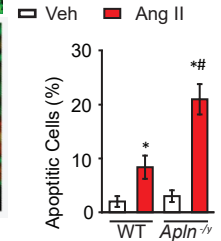
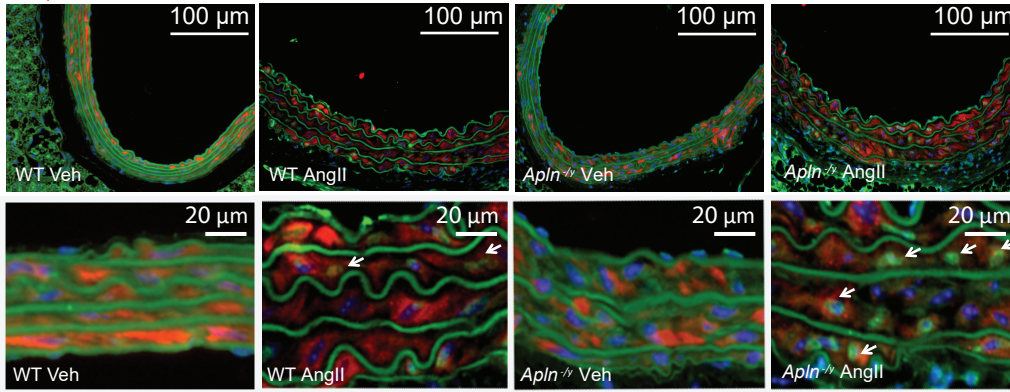


Figure S4. Phenylephrine (PE) results in equivalent blood pressure increase in WT and *Apln*^{-/-} mice without leading to abdominal aortic aneurysm formation. WT and *Apln*^{-/-} mice show similar baseline blood pressure (A), pulse pressure (B) and heart rate (C) during day time and night time as recorded in conscious mice by implanted telemetry probes; n=8 in each group. (D) Delivery of PE (40 mg/kg⁻¹d⁻¹) using mini-osmotic pump, resulted in a similar increase in blood pressure in *Apln*^{-/-} mice as induced by Ang II. Representative images (E) and quantification of ultrasound vasculography (F) revealed that PE treatment failed to change the aortic luminal size or result in AAA formation in *Apln*^{-/-} mice; n=8 in each group. Sys=systolic; Dia=diastolic; MABP=mean arterial blood pressure. *p<0.05 compare to day time.

A Abdominal aorta, 2 weeks
Calponin/TUNEL/Elastin/DAPI



B Abdominal aorta, 2 weeks
DHE/Elastin

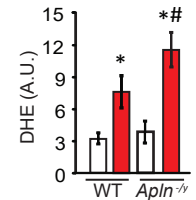
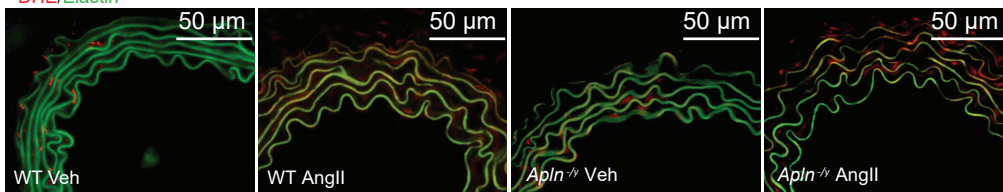


Figure S5. Loss of apelin exacerbates cell apoptosis and oxidative stress in the aortic wall in response to Ang II. (A) Representative images of TUNEL apoptosis staining on aortas. WT and *Apln*^{-/-} have minimal apoptosis at baseline; 2 weeks of Ang II treatment is sufficient to increase the apoptosis in *Apln*^{-/-} abdominal aorta compared to WT. Bottom panel are higher magnification with white arrows indicating TUNEL+ve cells. (B) Representative images of DHE fluorescence showing a similar trend to the observed apoptotic phenotype. Veh=saline; Ang II=angiotensin II; TUNEL=Terminal deoxynucleotidyl transferase dUTP nick end labeling; DHE=dihydroethidium. n=6 in each group. *p<0.05 compare to vehicle; #p< 0.05 compare to Ang II treated group.

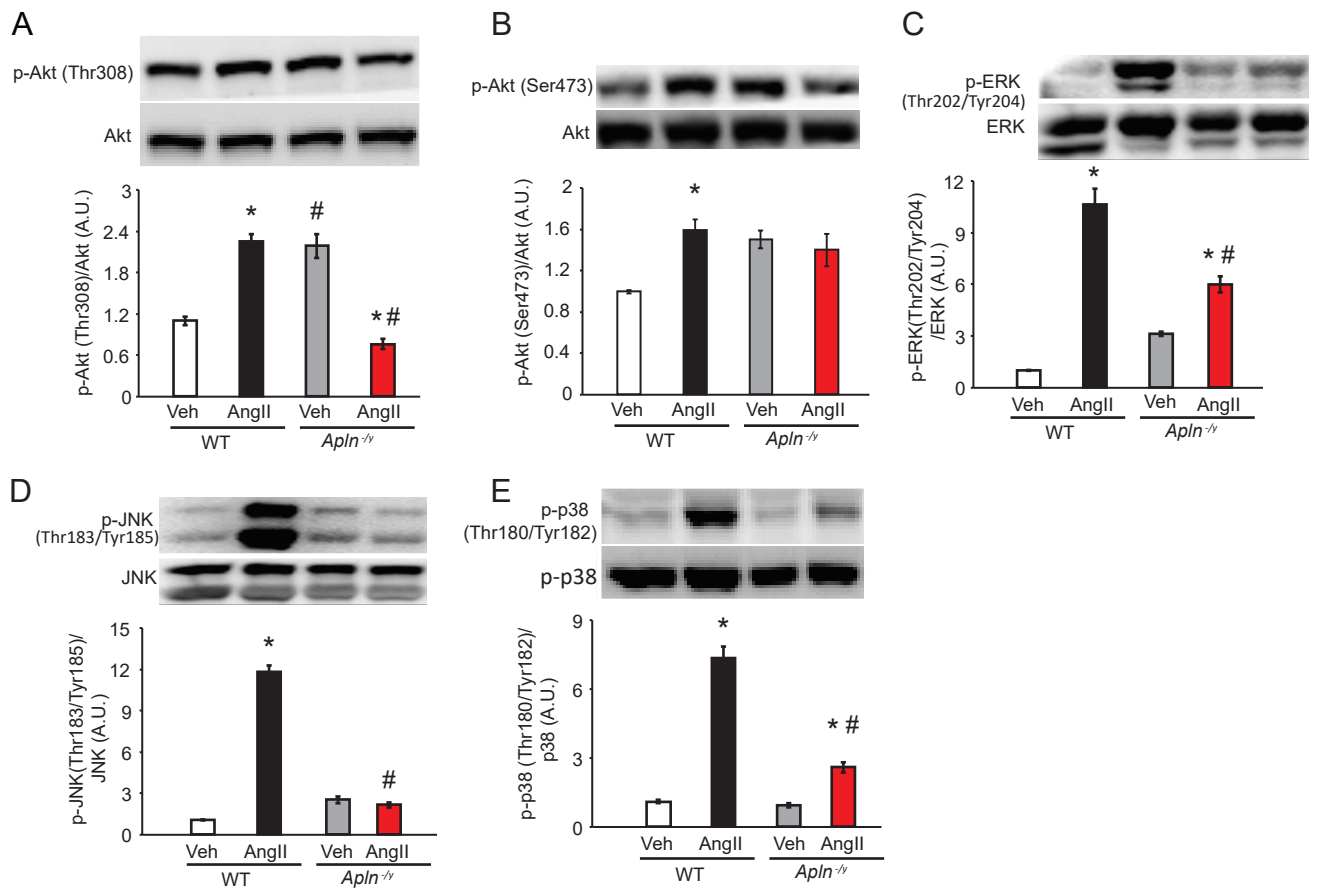


Figure S6. Western blot analysis of signaling pathways in the aorta. Representative immunoblots and quantification of changes in phosphorylated Akt, threonine-308-Akt (A), serine-473-Akt (B), phosphorylated Erk1/2 (C), JNK1/2 (D), and p38 (E) at baseline and following 2 weeks of vehicle or Ang II infusion in WT and *Apln*^{-/-} mice. n=4 in each group. *p<0.01 compared to vehicle group; #p< 0.05 compared to Ang II group.

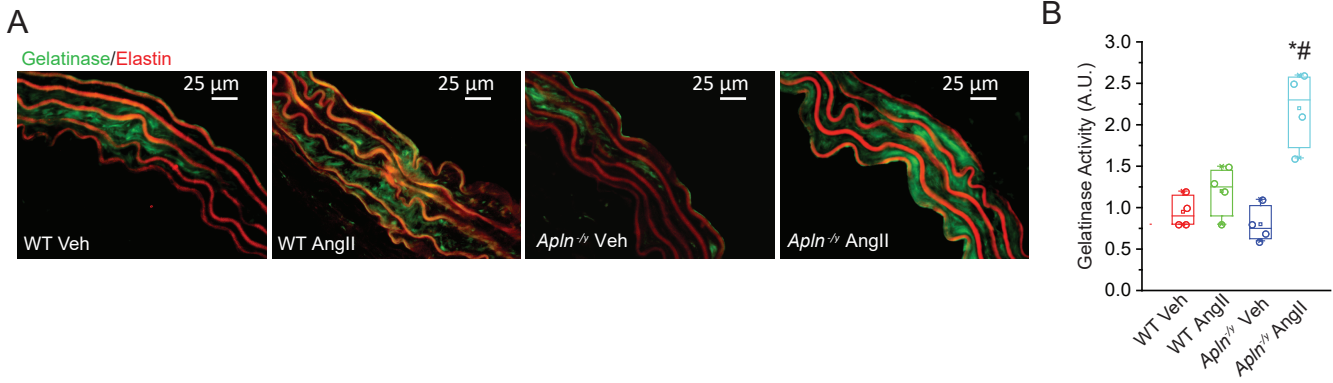


Figure S7. *In situ* zymographic analysis of gelatinase in aortas revealed that loss of apelin lead to greater increase in gelatinase activity in response to Ang II. Representative images of *in situ* zymography (A) and quantification (B) of gelatinase activity showing a dramatic increase in gelatinase activity in response to 2 weeks of Ang II infusion in *Apln*^{-/-} aortas compared to parallel WT aortas. Elastin has been pseudo-colored red to optimize the visual presentation; Veh=vehicle. n=4 per group. *p<0.05 compared to *Apln*^{-/-} vehicle; #p<0.05 compared to WT Ang II group.

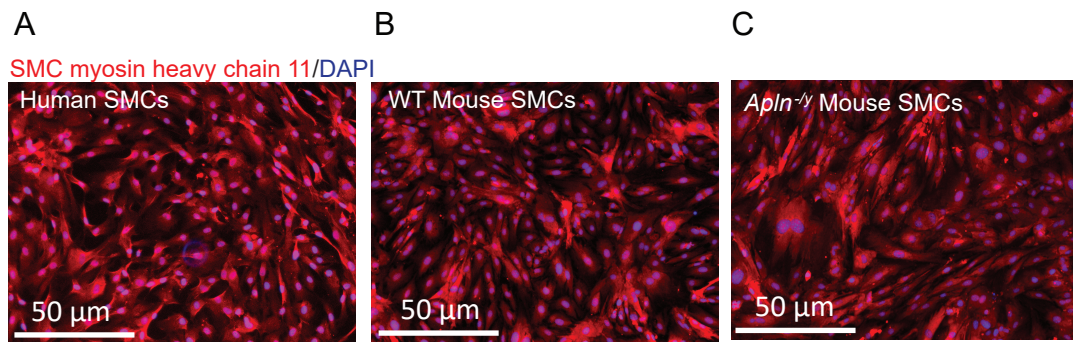


Figure S8. Isolated smooth muscle cells at passages 3 to 5 from human and murine (WT and *Apln*^{-/-}) aorta were characterized by immunofluorescence staining of smooth muscle myosin heavy chain 11, a specific marker for vascular smooth muscle cells (SMCs).

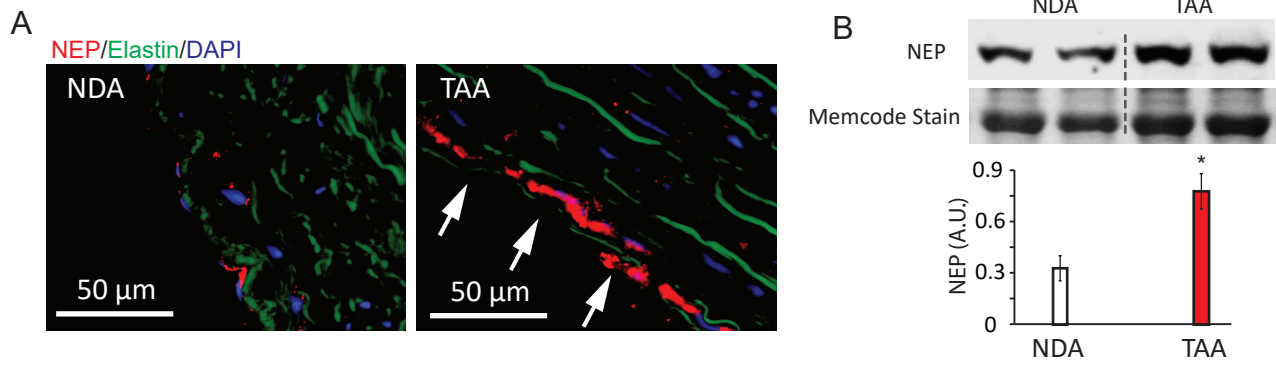


Figure S9. Neutral endopeptidase (NEP) is upregulated in aneurysmal thoracic aorta. (A) NEP immunofluorescent staining in NDA and TAA aortas revealed increased expression in NEP along the intima in TAA aortas. (B) Western blot analysis of NEP also demonstrates an upregulation of NEP in TAA aortas. NEP=nepriylisin or neutral endopeptidase; NDA=non-diseased aorta; TAA=thoracic (ascending) aneurysmal aorta. n=4 in each group. * $p < 0.01$ compare to NDA.

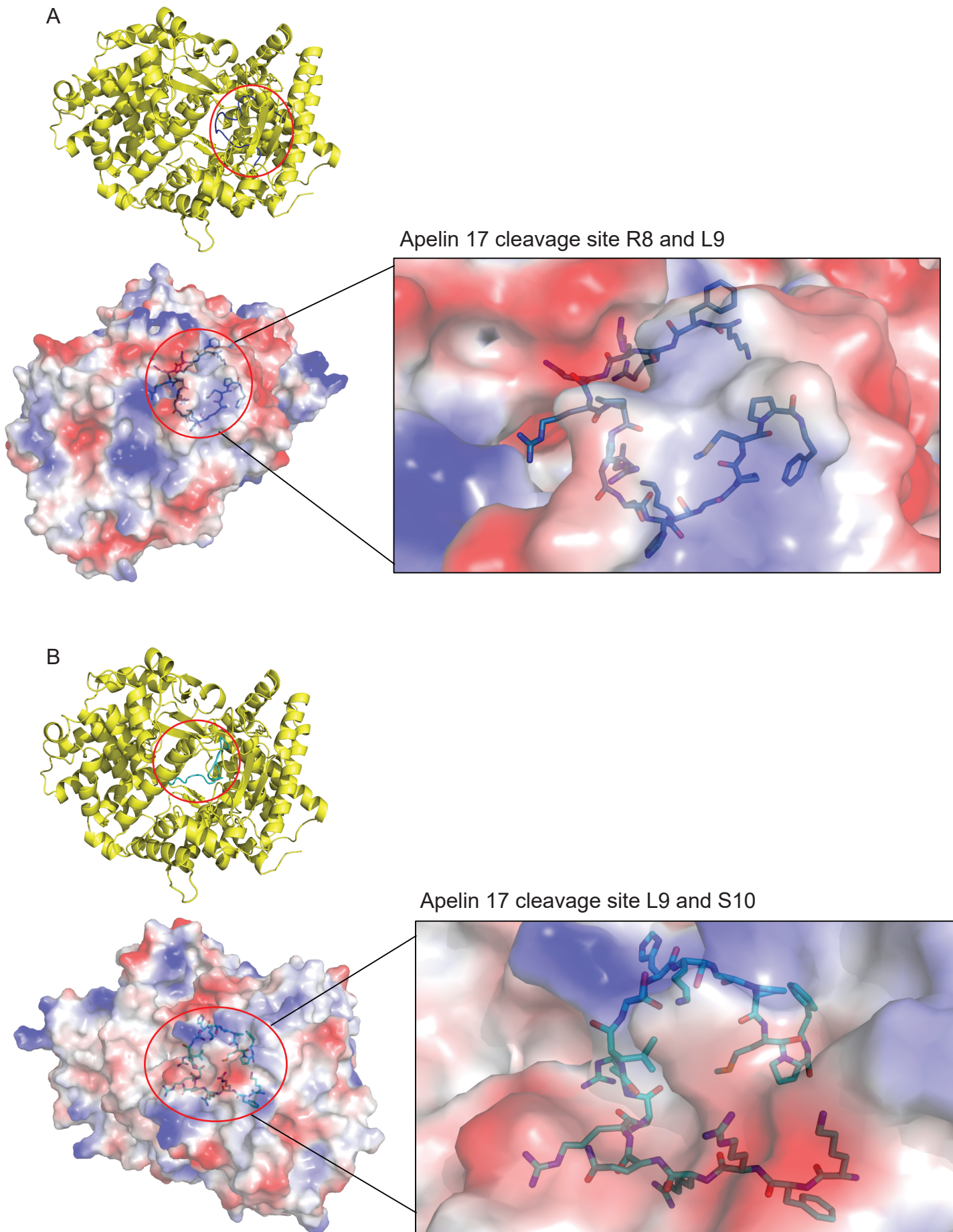


Figure S10. Modeling of the interactions between neutral endopeptidase (NEP) and apelin 17. NEP complexed with apelin 17 illustrating the arginine 8-lysine 9 cleavage site (A) and lysine 9-serine 10 cleavage site (B). The top panels illustrate the crystal structures of NEP while the electrostatic surface representations of NEP are shown in the bottom panels. NEP=neprilysin.

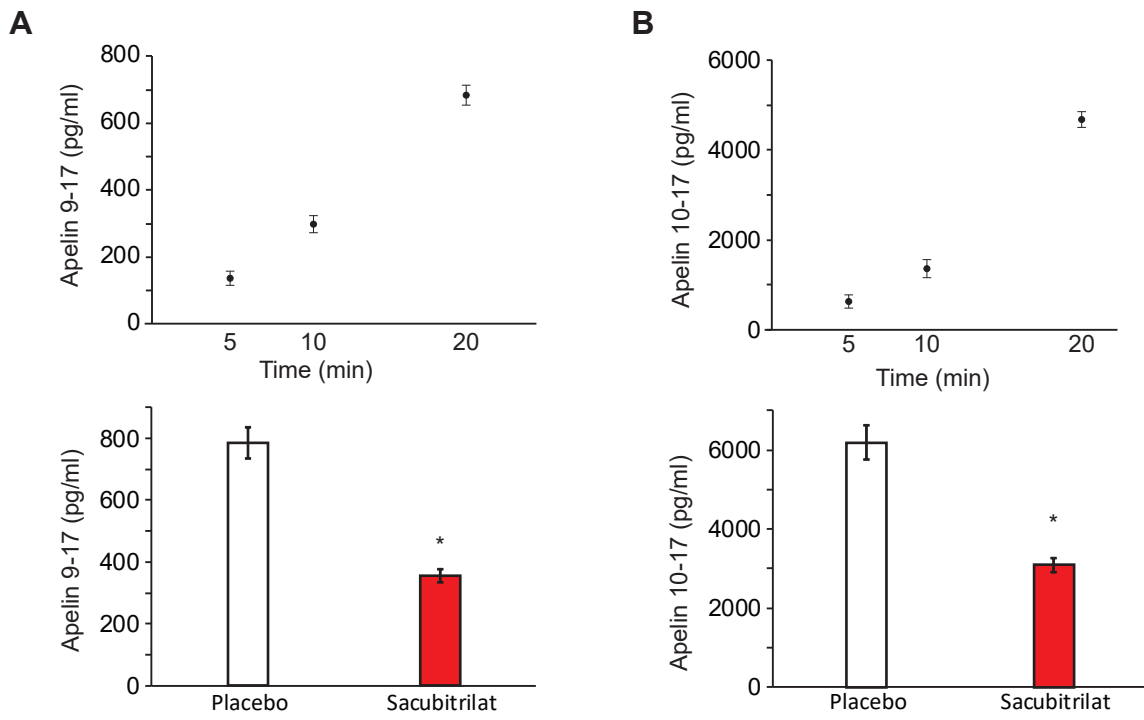


Figure S11. *In vitro* assay showing that apelin-17 can be cleaved by NEP in human plasma. Human recombinant NEP can cleave apelin-17 and generate apelin 9-17 (A) and apelin 10-17 (B) peptide fragments in a time-dependent manner (top panels). Sacubitrilat, a potent NEP inhibitor, can inhibit these cleavages and formation of peptide fragments (bottom panels). * $p < 0.01$ compared to placebo groups, $n = 3$ in each group.